ISTANBUL TECHNICAL UNIVERSITY ★ GRADUATE SCHOOL

FABRICATION OF SWCNT/AgNW/PEDOT:PSS NANOCOMPOSITE TRANSPARENT CONDUCTIVE FILMS

M.Sc. THESIS

Serra Melek AKYÜZ

Energy Science and Technology Division

Energy Science and Technology Programme

FEBRUARY 2022

ISTANBUL TECHNICAL UNIVERSITY ★ GRADUATE SCHOOL

FABRICATION OF SWCNT/AgNW/PEDOT:PSS NANOCOMPOSITE TRANSPARENT CONDUCTIVE FILMS

M.Sc. THESIS

Serra Melek AKYÜZ
(301171054)

Energy Science and Technology Division

Energy Science and Technology Programme

Thesis Advisor: Prof. Dr. Nilgün KARATEPE YAVUZ

FEBRUARY 2022

İSTANBUL TEKNİK ÜNİVERSİTESİ ★ LİSANSÜSTÜ EĞİTİM ENSTİTÜSÜ

KARBON NANOTÜP/GÜMÜŞ NANOTEL/PEDOT:PSS NANOKOMPOZİTLERDEN TRANSPARAN VE İLETKEN İNCE FİLMLERİN ÜRETİLMESİ

YÜKSEK LİSANS TEZİ

Serra Melek AKYÜZ
(301171054)

Enerji Bilim ve Teknoloji Anabilim Dalı

Enerji Bilim ve Teknoloji Programı

Tez Danışmanı: Prof. Dr. Nilgün KARATEPE YAVUZ

ŞUBAT 2022

Serra Melek AKYÜZ, a M.Sc. student of İTÜ Graduate School student ID 301171054 successfully defended the thesis entitled "FABRICATION OF SWCNT/AgNW/ PEDOT:PSS NANOCOMPOSITE TRANSPARENT CONDUCTIVE FILMS", which she prepared after fulfilling the requirements specified in the associated legislations, before the jury whose signatures are below.

Thesis Advisor :	**Prof. Dr. Nilgün KARATEPE YAVUZ** Istanbul Technical University	.....
Jury Members :	**Prof. Dr. Esra ÖZKAN ZAYİM** Istanbul Technical University	.....
	Prof. Dr. Serap GÜNEŞ Yıldız Technical University	.....

Date of Submission : 12 January 2022
Date of Defense : 11 February 2022

To my big AKYÜZ family,

FOREWORD

First and foremost, I would like to express my sincere gratitude to my advisor Prof. Dr. Nilgün K. YAVUZ, for her guidance, time and encouragement throughout my study.

I thank Prof. Dr. Esra ZAYİM ÖZKAN for letting me use her UV-VIS Spectrophotometer for my optical transparency measurements whenever I needed.

I thank Prof. Dr. Ayfer KALKAN BURAT, Ahu Galen ALTAŞ from TÜBİTAK MAM and Dr. Sinem BOZAR from Yıldız Technical University for providing me thionyl chloride, silver nanowires and PEDOT:PSS for my thesis, respectively.

I would also like to thank my close friends for always lending me a shoulder to lean on, for standing by me and for picking me up when I fall. They made my good times better and my hard times a whole lot easier. I will be forever grateful for their positive influence in my life.

Last but not least, I thank my family for their love and never ending support in all of my decisions. I feel so lucky to have such a wise and caring family who have always gone out of their ways to help me. Without their encouragement, I would never have come this far.

I am indebted to ITU BAP for their financial support in this study under the project code 42452.

January 2022

Serra Melek AKYÜZ
(Chemical Engineer)

TABLE OF CONTENTS

Page

ABBREVIATIONS

AFM : Atomic force microscope
AgNW : Silver nanowire
AuNW : Gold nanowire
AZO : Aluminum doped tin oxide
CNT : Carbon nanotube
CuNW : Copper nanowire
DCB : Dichlorobenzene
DI : Deionised water
DMF : Dimethylformamide
DMSO : Dimethyl sulfoxide
DOS : Density of states
DTG : Derivative Thermogravimetric analysis
FET : Field emission transistor
FTO : Fluorine doped tin oxide
HCl : Hydrochloric acid
ITO : Indium tin oxide
LCD : Liquid crystal display
m-SWCNT : Metallic single-walled carbon nanotubes
NMP : N -Methyl-2-pyrrolidone
NW : Nanowire
NW : Nanowire
OLED : Organic light-emitting diode
PDMS : Polydimethylsiloxane
PEDOT: PSS : Poly (3, 4-ethylenedioxithiophene): polystyrenesulfonate
PEG : Polyethylene glycol
PtNW : Platinum nanowire
PV : Photovoltaic
rGO : Reduced graphene oxide
SC : Sodium cholate
SDBS : Sodium dodecyl benzene sulfonate

SDS : Sodium dodecyl sulfate

SEM : Scanning electron microscope

s-SWCNT : Semiconducting single-walled carbon nanotubes

SWCNT : Single-walled carbon nanotube

TCE : Transparent conductive electrode

TCF : Transparent conductive film

TCO : Transparent conductive oxide

TGA : Thermogravimetric analysis

TMO : Transparent metal oxide

vHs : Van Hove singularities

XPS : X-ray photoelectron spectroscopy

SYMBOLS

a	**:** Absorption coefficient (cm^{-1})
c	**:** Speed of light (m/s)
e	**:** Elementary charge (C)
E_F	**:** Fermi energy level (eV)
E_g	**:** Band gap energy (eV)
E_p	**:** Plasmon (plasma) energy (eV)
$FeCl_3$	: Iron(III) chloride
F_{TC}	**:** Fraser's Figure of Merit
H_2SO_4:H_2O_2	**:** Piranha solution
HNO_3	**:** Nitric acid
I	**:** Intensity of incident light (W/m^2)
I_0	**:** Light intensity emitted through the thin film (W/m^2)
In_2O_3	**:** Indium tin oxide
In_2O_3	**:** Indium tin oxide
k	**:** Extinction coefficient ($M^{-1}.cm^{-1}$)
m*	**:** Effective mass of carriers
n	**:** Electrons
n,m	: non-negative integers
N_2	**:** Nitrogen
$Na_2S_2O_8$	: Sodium persulfate
p	**:** Holes
R_{sh}	**:** Sheet resistance (Ω/sq)
Sn_2O2:Al	**:** Aluminum doped tin oxide
Sn_2O2:F	**:** Fluorine doped tin oxide
$SOCl_2$	**:** Thionyl chloride
t	**:** Homogeneous thickness (nm)
T	**:** Optical transparency (%)
x	**:** Integer (~10)
$\vec{C}$	**:** Chiral vector

η : Carrier concentration (m^{-3})

σ : Electrical conductivity (S/cm)

θ : Chiral angle

ρ : Resistivity (Ω.m)

Φ_{FC} : Haacke's Figure of Merit

$\mu_{n,p}$: Carrier mobility ($m^2/(V \cdot s)$)

ω_p : Plasma frequency (s^{-1})

λ_p : Plasmon (plasma) wavelength (nm)

$\varepsilon_r\varepsilon_0$: Permittivity ($C^2/(N.m^2)$)

$\overrightarrow{\propto_1}$: Graphene vector 1

$\overrightarrow{\propto_2}$: Graphene vector 2

LIST OF TABLES

Page

LIST OF FIGURES

Page

FABRICATION OF SWCNT/AgNW/PEDOT:PSS NANOCOMPOSITE TRANSPARENT CONDUCTIVE FILMS

SUMMARY

Transparent conductive films have become critical components in modern devices due to rapid developments in science and technology. These devices range from touch screens to solar cells that reach out to a large proportion of the industry and our daily lives. To date, progress in nanotechnology has led to the discovery of unique nanomaterials such as carbon nanotubes, metal nanowires, and conductive polymers. These nanomaterials have sparked many researchers' attention towards extensive research. However, it has been determined that each material has a number of drawbacks as well as benefits that restrict its use in large-scale production processes. Thus, researchers have focused their efforts on developing nanocomposites consisting of different materials in order to overcome the limitations imposed by these single components.

The primary objective of this study is to develop nanocomposites that derive from SWCNTs, PEDOT:PSS and AgNWs to obtain highly conductive and transparent thin films. Highly conductive TCFs were prepared by dispersing SWCNTs in an NMP solution by spray coating method. Optoelectronic properties were studied by the effect of spray gun carrier gas pressure, concentration and volume sprayed onto the substrates. The prepared thin films were subjected to post treatments with nitric acid (HNO_3) using different treatment methods and times in order to improve the electrical conductivity. To further investigate the effect of p-doping in SWCNT thin films, HNO_3 treatments were combined with thionyl chloride ($SOCl_2$). The experimental results indicated that spray coating is an effective method to obtain highly conductive films without any chemical treatment, resulting in 273 Ω/sq sheet resistance, at 84 % in the visible range. Additionally, the optimized films treated with both HNO_3 and $HNO_3/SOCl_2$ showed great improvements at 83% - 85 % in the visible range and in sheet resistances followed by 98 Ω/sq and 103 Ω/sq with very good FOM values (1.6×10^{-3} and 2×10^{-3}, respectively). The SWCNT films were introduced to different PEDOT: PSS dispersions (PH 1000, PH 500, Clevios FET) and thin films were fabricated with the spin coating method. Sheet resistance and optical transparency measurements of the films with different PEDOT: PSS solutions were evaluated, and the film quality of the films was also taken into consideration in determining the optimum concentration. The effect of DMSO on the overall conductivity of SWCNT/PEDOT: PSS thin films was also investigated in this thesis. As a result of these investigations, Clevios FET dispersions showed better film performance while the high acidity of PH 1000 and PH500 deteriorated the SWCNT film surface during spin coating fabrication. The sheet resistance of SWCNT/FET film was measured as 142 Ω/sq with a transmittace of 55%. Additionally, the DMSO post-treatments were found to be effective to decrease the sheet resistance of films fabricated using PH 500 dispersions, while the SWCNT/FET films were negatively impacted by the treatment. The inverse effects of the post-treatment method can be explained by the differences

in PH 500 and Clevios FET's morphological structures and can be matched with other studies in the literature. The addition of AgNWs were incorporated into SWCNT and PEDOT:PSS inks using two different wet coating techniques. For the first strategy, the AgNWs were added to the PEDOT: PSS dispersion, and the SWCNT/PEDOT:PSS-AgNW nanocomposites were fabricated by the spin coating method. In the second approach, AgNWs were mixed into the SWCNT ink and films fabricated by the spray coating method. The PEDOT:PSS dispersion was spin coated in the final assembly of SWCNT-AgNW/PEDOT:PSS films. The addition of AgNWs did not result in a significant decrease in sheet resistance with either approach. The high surface resistance can be associated with the AgNWs' low electrical conductivity due to their low aspect ratio, bulk impurities, and/ or acid corrosion of AgNWs lead by PEDOT:PSS. SWCNT-AgNW/PEDOT:PSS nanocomposite made with the second method showed the best performance among these two methods, where the resistance of the film was measured as 220 W/sq with a 55% transmittance.

KARBON NANOTÜP/GÜMÜŞ NANOTEL/PEDOT:PSS NANOKOMPOZİTLERDEN TRANSPARAN VE İLETKEN İNCE FİLMLERİN ÜRETİLMESİ

ÖZET

Transparan ve iletken ince filmlere (TCF) karşı duyulan ilgi dokunmatik ekranlar, katı hal aydınlatma teknolojileri, organik ışık emisyonu (OLED), fotovoltaik güç sistemleri gibi optoelektronik cihazların hayatımızda önemli hale gelmesiyle gitgide artış göstermiştir. TCF teknolojisi günümüzde optoelektronik ve fotovoltaik uygulamalarda kullanılmasının yanı sıra antistatik ve elektromanyetik girişim koruma sağlama görevi gören cam kaplamaları alanlarında da kullanılmaktadır. Bunun yanında, otomobil ve uçak kokpitlerinin cam panellerinde buz çözme amaçlı olarak kullanılan ısıtma elemanları uygulamaları da literatürde sıkça rastlanabilir. Teknolojiye olan talebin hızla artmasıyla gelecekte de TCF üzerinde yapılan çalışmaların çok daha fazla artması öngörülmektedir. TCF'lerin uygulama alanlarına göre parametreler değişmektedir. Örneğin, TCF'lerin düşük yüzey dirence ve iyi ısıl iletkenliğe sahip olması termal uygulamalarda, yüksek optik geçirgenlik özelliği göstermesi ise otomobil ve kokpit camlarında kullanılmasını mümkün kılmıştır. TCF için kullanılan malzemeler görünür dalga boylarında iyi optik geçirgenliği gösteren ve yüksek derecede elektriksel iletkenliğe sahip malzemeler sınıfını temsil etmektedir.

Katkılı metal oksit grubunda olan indiyum kalay oksit (ITO), günümüze kadar TCF nanomateryalleri arasında literatürde en popüler çalışılan ve endüstrideki TCF uygulamalarında en yaygın kullanılan malzemelerden bir tanesi olmuştur. Yaklaşık % 90 optik geçirgenliğe ve < 100 Ω/kare yüzey direncine sahip olan ITO, geçmişte yapılan çalışmalarda ve optoelektronik endüstrisinde tercih edilme sebebi olmuştur. Bununla birlikte, ITO'nun birtakım dezavantajları bulunmakta ve bu sebeple yeni nesil teknolojiye ayak uyduramamaktadır. Bunlardan birincisi indiyumun dünya üzerinde nadir bulunması ve indiyim kalay oksit filmin yüksek sıcaklıklarda litografik modelleme gibi karmaşık üretim süreci içerdiğinden maliyetinin son derece yüksek olmasıdır. İkinci en büyük dezavantajı ise mekanik dayanıklılığının son derece düşük olmasıdır. Kırılgan yapısı, esnek TCF uygulamalarını ve geniş yüzey uygulamalarını kısıtlamakta, bükülmeyi ve esnemeyi içeren dokunmatik ekran uygulamalarında çatlamaya yol açmaktadır. ITO'nun polietilen tereftalat (PET) altlığa kaplanmış filmlerin elektriksel iletkenlikleri, cam altlığa kaplanmış filmlerden yaklaşık 5 kat daha düşüktür. Bu sebeple araştırmacılar ITO'nun sahip olduğu açıkları kapatacak, ucuz maliyetli, nano ölçekli yeni malzemeler bulma arayışına başlamışlardır. Son yıllarda, nanoteknolojideki hızlı gelişme, farklı özelliklere sahip nanomalzemelerin sentezlenmesi için yeni fırsatlar sunmuştur. Metal oksit nano partiküller, karbon yapılı nano malzemeler, metal nanoteller ve yüksek elektriksel iletkenlik gösteren polimerler gibi malzemelerin kullanımıyla bu alanda pek çok gelişme meydana gelmiştir.

İyi mekanik esnekliğe sahip, yüksek optik geçirgenlik ve elektriksel iletkenliği olan grafen ve karbon nanotüpler (KNT'ler) gibi karbon yapılı nanomalzemeler, TCF'ler

için son derece uygundur. Karbon yapılı malzemeler arasından KNT'ler, kolay ve ucuz üretimi, ayarlanabilen benzersiz elektronik yapısı ve kuru/ıslak kaplamalarda gösterdiği uyumluluğundan dolayı diğer nanomalzemeler arasından sıyrılmış ve bu sebeple literatürde çok popüler bir malzeme haline gelmiştir.

PEDOT: PSS. Poli (3,4-etilendioksitiyofen): poli-(stirensülfonat) iletken bir polielektrolit kompleksidir. Günümüzde PEDOT: PSS çoğu laboratuvarlarda yaygın kullanılan bir nanomalzeme haline gelmiştir. Sulu çözeltilerindeki PEDOT ile PSS'in oranlarına göre yaklaşık 25 farklı formülasyonu mevcut bir şekilde ticari olarak satılmaktadır. Bu oranın değişimine göre iletkenlik artmaktadır. İnce film organik optoelektronik ve fotovoltaik cihazlarda, boşluk taşıyıcı tabaka (HTL) ya da transparan elektrot olarak yaygın kullanılmaktadır. Bu özelliklerinin yanında, geniş yüzey alanı gerektiren TCF uygulamalarında kolay kaplanma özelliğinden dolayı tercih edilmektedir. Yaygın bulunan bir malzeme olması nedeniyle de birçok yayına konu olmuştur. Elschner ve ark. tarafından 2010 yılında üretimi kapsamlı olarak incelenmiştir. ITO, KNT ve metal nanotel gibi yüksek yüzey pürüzlülüğüne sahip TCF malzemeleriyle pürüz azaltıcı ve koruyucu bir kaplama olarak da görev görmektedir.

Bu malzemelerin yanısıra, metal nanotel ağları ve metal nanogridler gibi nanoyapılar, TCF'lerde benzersiz optoelektronik özellikleri ve potansiyel uygulamaları nedeniyle büyük ilgi görmektedir. Metal nanotel ağları genellikle sol-jel metoduyla oluşturulur, bu sayede üretim maliyeti son derece düşüktür. Sol-jel metoduyla üretilen boy/en oranı yüksek gümüş nanoteller (AgNW'ler), yüksek optoelektronik performansa sahip TCF'ler üretmek için ideal bir prosestir. AgNW elektrodunun yüzey direnci ve görünür bölgedeki optik geçirgenliği, ITO elektrodunun özelliklerine çok yakındır.

ITO'da olduğu gibi, TCF'lere alternatif olarak yukarıda sıralanan malzemelerin dezavantajları bulunmaktadır. Örneğin KNT'lerin yan duvarlarında içerdikleri Van der Waals kuvvetleri, nanotüplerin birbirine yapışarak aglomerasyonuna yol açmakta ve çözücü içerisindeki dispersiyonlarını zorlaştırmaktadır. Öte yandan iletken polimerler arasından PEDOT:PSS ise, ortalama 1.5-2.5 pH seviyesine sahip yüksek asiditesi sahip olduğundan farklı malzemelerle birlikte kullanıldığında asit korozyonuna yol açmaktadır. Bunun yanısıra PEDOT:PSS higroskopik özellikte olup havada var olan nemi tutmaktadır. Bu durum ise PEDOT:PSS ince filmlerinin ortam koşullarına karşı son derece dayanıksız hale getirmekte ve buna bağlı olarak zamanla yüzey dirençlerinin yükselmesine sebep olmaktadır. AgNW filmlerinin en büyük eksiklikleri ise, pusluluklarının yüksek olması ve Ag elementinin pahalılığıdır. Bu bulgular sonucunda nanomalzemelerde sıkça görülen dezavantajlar, araştırmacıları nanokompozit yapılar oluşturmaya yönelik çalışmalar yapmaya itmiştir. Böylelikle malzemelerde yaşanan problemler farklı malzemelerle güçlendirilerek bir çözüm yolu aranmıştır.

Tez çalışmasının amacı, tek duvarlı karbon nanotüp (TDKNT), AgNW ve PEDOT:PSS kullanarak yüksek iletkenlik ve optik geçirgenliğe sahip ince filmler üretmek olmuştur. Üretilen nanokompozit filmlerin optoelektronik cihazlara uygun, dayanıklı ve yüksek film kalitesinde olması hedeflenmiştir. Nanokompozit ince filmler üretilmeden önce her 3 malzemenin optimizasyon çalışmaları yapılmıştır. Üretilen nanokompozit filmlerin en alt katmanında yer alan TDKNT'ler sprey kaplama yöntemiyle kaplanmıştır. Yüksek performanslı TDKNT'li filmleri üretmek farklı başlıklarda incelenerek bu filmlerin optoelektronik özellikleri karşılaştırılmıştır. Kaplama öncesi ticari Tuball TDKNT'ler 3 M'lik nitrik asit (HNO_3) çözeltisinde 3 saat boyunca kaynatılarak saflaştırılmıştır. Bu sayede TDKNT'ler metal

safsızlıklarından arındırılmıştır. 1.5x1.5 cm boyutunda kesilen cam altlıklar ise 3 farklı çözücü ile ultrasonik banyoda temizlendikten (izopropil alkol, etanol ve deiyonize su) sonra kurutularak UV–ozon cihazında bekletilmiştir. Temiz camlara hidrofilik özellik kazandırmak için pirana (H_2SO_4:H_2O_2, 3:1) çözeltisinde 9 dakika boyunca bekletilmiş, ardından bol deiyonize su (DI) ile yıkama yapılarak azot (N_2) tabancasıyla dikkatlice kurutulmuştur. Kurutulan camlar 200 °C'ye ayarlı ısıtıcılara yerleştirilerek TDKNT'li filmlerin kaplamaları yapılmıştır. Bu kaplamalarda TDKNT konsantrasyonu etkisine ek olarak, sprey kaplama yönteminde püskürtme basıncının ve kullanılan hacmin optoelektronik özelliklere etkisi incelenmiştir. Yapılan çalışmalar doğrultusunda en iyi optoelektronik özelliklere sahip TDKNT'li filmlerin 0.1 mg/ml konsantrasyonuna sahip, optimum çalışma basıncı 2 bar olan ve 1.5 ile 2 ml sprey kaplama hacmi kullanılan filmler olduğu saptanmıştır. Bu optimizasyonlarla üretilen TDKNT'li filmlerin yüzey direnci ortalama 200-700 Ω/sq aralığında ve görünür bölgede %70-89 optik geçirgenliğe sahip olduğu ölçülmüştür. Bu filmlerin yüksek yüzey dirençlerini düşürmeye yönelik HNO_3 ve tiyonil klörür ($SOCl_2$) ile kimyasal iyileştirmeler yapılmıştır. Nitrik asit muamelesi, 14.3 M ile gerçekleştirilmiştir. HNO_3 çözeltisi ile iyileştirilmeler, farklı yöntemlere (bekletme ve damlatma) bağlı olarak üretilen filmlerin elektronik özelliklerine ve film kalitelerine olan etkileri incelenmiştir. Bekletme sonrası filmler deiyonize suyla yıkanarak 80°C'deki etüvde kurutulmuştur. HNO_3 çözeltisinde bekletilen TDKNT'li filmlerin yüzeylerinin damlatma işlemine kıyasla daha çok zarar gördüğüne ve damlatma işleminin en az çözeltide bekletmek kadar efektif olduğuna dair bulgular elde edilmiştir. Damlatma yönteminde 14.3 M HNO_3 çözeltisinin iyileştirme süreleri de ele alınarak filme olan etkileri incelenmiş, bu işlem sonrası ek olarak $SOCl_2$ ile de muamele edilmiştir. Bu kapsamda, farklı sürelerde nitrik asit uygulanan filmler 97%'lik $SOCl_2$ çözeltisinde 30 dakika boyunca bekletilmiştir. İyileştirme sonrası elde edilen filmler N_2 tabancası ile kurutulmuş ve Raman spektroskopisi, taramalı elektron mikroskobu (SEM) , atomik kuvvet mikroskobu (AFM) ve dört noktalı prob ile karakterize edilmiştir. Yapılan analizlerle, HNO_3 ve/veya HNO_3/$SOCl_2$ kullanılarak uygulanan kimyasal işlemlerin TDKNT'li filmlerin yüzey dirençlerini etkili bir şekilde düşürdükleri gözlemlenmiştir. Bu filmlerin performansları Figure of Merit (FOM) hesabıyla literatürdeki yapılan diğer çalışmalarla karşılaştırılmış, bu tez çalışmasındaki üretilen filmlerin (8.2×10^{-4} ile 2×10^{-3}) performanslarının daha üstün olduğu görülmüştür. TDKNT'li filmlerin optimizasyonu sonrası iletken polimer ile nanokompozit film çalışmaları yapılmıştır.

PEDOT:PSS çalışmalarında farklı dispersiyonlar (PH1000, PH500, FET) kullanılmış, bu dispersiyonların filmin optoelektronik özelliklerine ve kalitesine olan etkisi incelenmiştir. Yapılan çalışmalar sonucu PH 1000'in yüksek asiditesi yüzünden TDKNT'li filmlerin yüzeylerini HNO_3 ile yapılan kimyasal iyileştirmelerdeki gibi zarar verdiği gözlemlenmiştir. Buna ek olarak ticari PEDOT:PSS'in mavi rengi TDKNT'li filmlerin optik geçirgenliğinde büyük bir düşüşe sebep olmaktadır. Bu nedenlerden ötürü dispersiyon olarak FET seçilerek optik geçirgenlikteki düşüşü önlemek için FET dispersiyonları 1:1 oranında DI su ile seyreltilmiştir. Ayrıca, Clevios PH 500 ve FET ile hazırlanan TDKNT/PEDOT:PSS'li ince filmlere dimetil sülfoksit (DMSO) ile kimyasal iyileştirmeler yapılmıştır. PH 500 ile yapılan filmlerin yüzey direncinde etkili bir düşüş görüldüğü fakat film kalitesinin düştüğü, FET ile yapılan filmlerde DMSO katkısının PH 500'deki kadar etkili olmadığı ve yüzey direncini yükselttiği görülmüştür. DMSO katkısının PEDOT:PSS zincirlerinde faz ayrımı yaptığını, PH 500 ve FET dispersiyonlarına ait ortalama tanecik boyutlarının birbirinden farklı olduğunu ve bu durumun DMSO konsantrasyonu ile ilişkili olduğu

sonuçlarına varılmıştır. Tüm bulgular değerlendirildiğinde, PEDOT:PSS dispersiyonları arasından Clevios FET, TDKNT yüzeyine zarar vermeden kolayca kaplandığı için nanokompozit çalışmalarında tercih edilmiştir. Clevios FET ile oluşturulan en başarılı TDKNT/PEDOT:PSS filmin 142 Ω/sq ve 55 % optik geçirgenlikte olduğu tespit edilmiştir.

AgNW'ler, hazırlanan TDKNT/NMP ya da PEDOT:PSS/DI dispersiyonuna ilave edilerek 2 farklı yöntemle nanokompozitler üretilmiştir. Bu iki farklı stratejinin uygulanma amacı, AgNW'nin iki farklı malzeme içerisindeki gösterdiği performans ve film formasyonunun incelenip karşılaştırılmasıdır. İlk yöntemde, 0.05 mg toz AgNW FET dispersiyonuna eklenerek karıştırılmış ve üretilen TDKNT'li film üzerine dönel kaplama yöntemiyle kaplanarak nanokompozit TDKNT/PEDOT:PSS-AgNW filmleri oluşturulmuştur. İkinci yöntemde ise ilk yöntemdeki gibi aynı miktarı içeren toz AgNW'ler santrifüj sonrası elde edilen TDKNT/NMP çözeltisine eklenerek sprey kaplama yöntemiyle temiz cam substratlar üzerine kaplanmıştır. Üretilen TDKNT/AgNW filmlerin üzerine ise FET dönel kaplama yöntemiyle kaplanmış, TDKNT-AgNW/PEDOT:PSS filmleri oluşturulmuştur. Her iki yöntemle üretilen nanokompozit yapılı filmlerden beklenen düşük yüzey direnci ölçülememiştir. Yüksek yüzey direnci AgNW'lerin düşük boy uzunlukları ve safsızlıklarından ötürü düşük elektriksel iletkenliğe sahip oldukları ve AgNW'lerin ilk yapılan yöntemde PEDOT:PSS'in yüksek asiditesi sebebiyle boylarının daha fazla kırıldığı sebepleriyle açıklanabilmektedir. Bu iki yöntem arasında en iyi performansı ikinci yöntemle yapılan TDKNT-AgNW/PEDOT:PSS nanokompozit göstermiş olup, filmin direnci 220 Ω/sq, optik geçirgenliği ise görünür bölgede % 60 olarak ölçülmüştür.

1. INTRODUCTION

Transparent conductive films (TCFs), in other words, transparent conductive electrodes (TCEs) are essential components in various complex technological areas such as liquid crystal displays on mobile phones and screens, flat panel displays and transparent heaters along with new emerging technologies namely organic light-emitting displays (OLED), photovoltaic devices (PV), or transparent field-effect transistors (FETs). Owing to its name, TCFs are thin films made out of organic or irorganic nanomaterials that possess electrical conductivity with optical transparency. The most widely used TCF material in industry is known to be an inorganic nanomaterial, namely indium tin oxide (ITO), which is grouped as transparent conductive oxides (TCOs). ITOs low sheet resistance (20-100 Ω/sq) along with its high transparency (~90%) within the range of 100-400 nm thickness makes a perfect candidate for most applications for TCFs. However, due to the limitation and expense of indium on earth, high costs of fabrication and poor physical properties of ITO , has made it a less desirable material for large-scale, flexible and cost-effective TCFs.

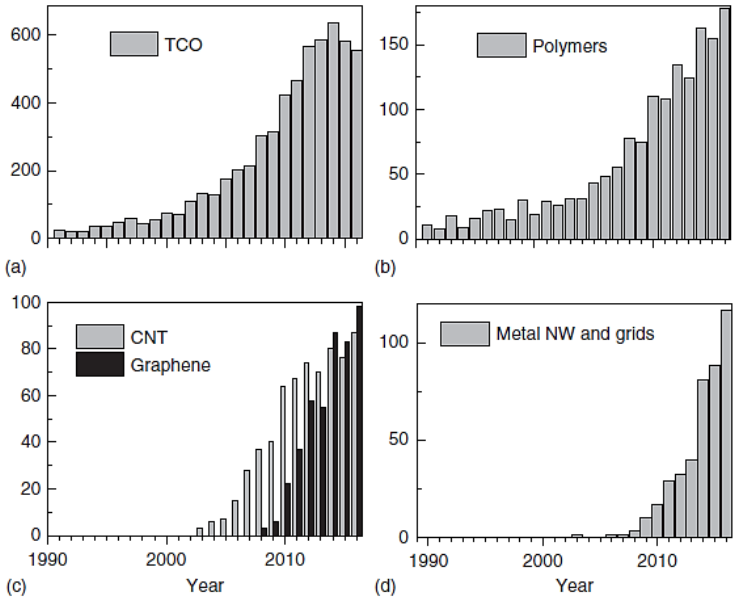

Figure 1.1 : Publications per year between 1990-2016 on TCF materials: (a) TCOs, (b) polymers, (c) carbon-based and (d) metal-based nanomaterials [1].

Consequently, publications towards ITO have diminished, while alternatives such as carbon- and metal-based nanomaterials and conductive polymers have won researchers' attention and are taking relevance in TCF literature, as demonstrated in Figure 1.1. There have been numerous studies done on single-walled carbon nanotubes (SWCNTs), as opposed to carbon-based materials, due to its relatively cheaper production cost than ITO. Previous studies have shown poly(3,4-ethylenedioxythiophene) polystyrene sulfonate (PEDOT:PSS) to be a standard chemical due to its ease of processability as a TCF material and can be found in many formulations with a variety of solid content up to 25 types of dispersions. Another interesting alternative is silver nanowires (AgNWs) which show very similar optoelectronic properties to ITO, with sheet resistance ranging from 1-100 Ω/sq approximately under 100 nm thickness and optical transparency value approximately 80-90% in the visible spectrum. In addition, AgNWs compatibility with any substrate material and cost-effective wet coating methods such as spray, spin and dip coating makes them an excellent candidate for future flexible electronics.

However, the moderate conductivity of SWCNTs and PEDOT:PSS possess is not enough to replace ITOs performance. Moreover, PEDOT:PSS has stability issues when exposed to light and air, which diminishes its lifespan. Although AgNWs have excellent optoelectronic properties to serve as a substitute for ITO, their adhesion and high surface roughness in wet coatings limit their applications in commercial areas. Given the inherent disadvantages of each material, researchers have concentrated their efforts on developing nanocomposites composed of these materials in order to overcome the constraints that these individual materials impose. Nanocomposites offer great advantages for future technologies by developing innovative materials. The incorporation of different nanomaterials allow to fine-tune the optoelectronic properties, along with imparting with additional features to the composites such as mechanical strength and high stability.

The major objective of this thesis study is to fabricate nanocomposites using SWCNTs, AgNWs and PEDOT:PSS as nanomaterials to obtain highly transparent and conductive thin films. Moreover, this thesis aims to contribute to the literature in the field of nanocomposites by comprehensively investigating factors that affect film quality, conductivity and transparency of the fabricated thin films.

The thesis is divided into 5 chapters. An overview of TCFs and their important parameters are given in Chapter 2.

Chapter 3 provides a detailed background of the electrical and optical properties of the TCF materials used in this thesis, namely SWCNTs, PEDOT:PSS and AgNWs, along with the film fabrication methods.

The experimental procedures to fabricate SWCNTs and the nanocomposites are given in Chapter 4 in great detail. The methodology starts from purification and dispersion of the commercial Tuball SWCNTs. Then, effects of the spray coating technique are investigated by several influencing parameters, including the concentration of SWCNT in N-Methyl-2-pyrrolidone (NMP), the gas pressure of the spray coating gun and the volume used during fabrication. Chemical post treatment methods were employed to the SWCNTs to enhance their conductivity with different doping methods and treatment times of nitric acid (HNO_3). To further investigate the effect of p-doping in SWCNT thin films, HNO_3 treatments were then combined with thionyl chloride ($SOCl_2$). Different types of PEDOT:PSS dispersions (PH 1000, PH 500 and Clevios FET) were spin coated onto the SWCNT films and their optoelectronic properties were compared to optimize the concentration of PEDOT:PSS ink. Furthermore, the effect of dimethyl sulfoxide (DMSO) was investigated to increase the electrical conductivity of SWCNT/PEDOT:PSS films. The addition of AgNWs were incorporated into SWCNT and PEDOT:PSS inks using 2 different wet coating techniques. For the first strategy, AgNWs were added into PEDOT:PSS ink followed by spin coating on top of the SWCNT film for the nanocomposite fabrication. The resulted fabrication formed SWCNT/PEDOT:PSS-AgNW nanocomposites. The second strategy was conducted by the addition of AgNWs into the SWCNT/NMP ink. Thin films of SWCNT-AgNWs were fabricated using spray coating method and the PEDOT:PSS solution was spin coated as a top layer to form SWNCT-AgNW/PEDOT:PSS nanocomposites.

Chapter 5 compares and contrasts the findings of this research with other studies as well as within the chapter itself. Thermogravimetric and derivative thermogravimetric analysis of the SWCNT powder, surface tension properties of the glass substrate and effects of spray coating parameters, concentration of the SWCNT dispersion and post treatment results are throurougly discussed. Thermogravimetric (TGA) and derivative thermogravimetric analysis (DTG) of the SWCNT powder, surface tension properties of the glass substrate, effect of spray coating parameters, concentration of the SWCNT

dispersion, and post treatment results are thoroughly discussed. All SWCNT films are characterized by SEM, AFM, and post-treated films were investigated through Raman spectroscopy.

Furthermore, the physical characteristics different dispersions of PEDOT: PSS/deionised water (DI) are evaluated, and the results of DMSO-treated films are presented. The provided AgNW powder's EDX and SEM analysis results are also given and discussed. SWCNT/PEDOT:PSS-AgNW and SWCNT-AgNW/PEDOT:PSS TCF performances were compared each other by sheet resistance and optical transparency measurements. The optoelectronic properties of all films were measured by Keitley 2400 Source Meter and UV-Vis Spectrophotometer.

The final part contains the conclusions of this thesis that provides a summary of all results while the recommendations section presents helpful insights for future studies of nanocomposites.

2. TRANSPARENT CONDUCTIVE FILMS

Transparent conductive films or transparent conductive electrodes are components in various information (namely displays) and energy technologies, which transmit light, mostly in the visible range, and conduct electrical current at the same time. These films play an essential role in technologies that have became predominant in our daily life, like touch panels on mobile phones, tablets and liquid crystal displays (LCDs), or in emerging new technologies namely PVs, transparent heaters, OLEDs, capacitors and FETs.

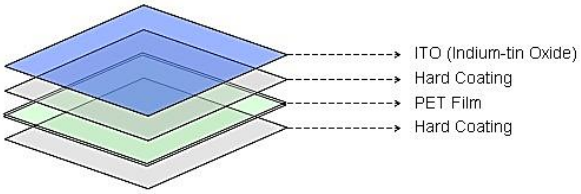

Figure 2.1 : Composition of ITO coated thin film by Kaivo Electronic.

Figure 2.1 represents a scheme of a thin film. A TCF's working principle in an optoelectronic device can be described as a window, which allows light to enter and leave while extracting electrons or holes in the active layer of the component. In this regard, essential requirements of a TCF device is to possess high conductivity or low sheet resistance along with high optical transparency in the visible range.

To date, transparent metal oxides (TMO) or transparent conductive oxides (TCOs) has acclaimed wide popularity in the research field of TCFs due to their excellent optoelectronic properties. Indium tin oxide (In_2O_3 ,ITO), aluminum doped tin oxide (SnO_2:Al**,** AZO) and fluorine doped tin oxide (SnO_2:F**,** FTO) have been studied and refined for years, which resulted in widespread use in various devices. This began in 1930 at the Corning research facilities with, coincidental discovery of novel transparent conductive oxide particles [14]. Metal oxides, especially mixtures with indium and tin oxides, were further investigated in the 1940s, [15]. Later on, these studies were focused on device fabrication when advances in technology made it possible to fabricate thin films of TCOs.

ITO has been the most popular material within TCO nanomaterials since the 20th century. The most prominent features of ITO can be identified as having low sheet resistance in approximately 20-100 Ω/sq with film thicknesses ranging from 100 to 400 nm and high transparency (~80-90%) in the visible range of the spectrum. Studies reaching back to 1947 with its first patent, made it an extremely mature material in the TCF field. Therefore ITO has been the most demanded nanomaterial for touch screen, liquid crystal display and photovoltaic applications. Nevertheless, drawbacks such as unavailability of indium element, high production costs and poor mechanical properties of ITO thin films limit its use in future nanoelectronics. Specifically, since ITO is a ceramic material, its brittleness towards low strains makes it undesirable not only in consumer products such as touch screens of mobile phones and tablets, but also in emerging technologies such as photovoltaics. The brittle nature of ITO causes small cracks on the thin film surface, which results in deterioration in film quality, decrease in conductivity and reduced lifespan.

The shortcomings of ITO has pushed forward the investigation into other promising materials in the field of TCFs, namely carbon nanotubes, graphene, conductive polymers, metallic grids and nanowires. Among these carbon- based materials, especially carbon nanotubes (CNTs) stimulated popularity and extensive research among academic and industrial fields since their discovery in 1990 by Sumio Iijima . Even though the early studies of CNTs were focused on nanotube growth and characterization, later studies attracted attention in application developments as a result of their excellent mechanical and chemical stability and good electrical conductivity. The list of applications for CNTs include: heating elements [16], [17] , transistors [18], [19], actuators [20], field emission devices [21]–[23], capacitors [24], chemical sensors [25]–[27] etc. What makes CNTs application range so wide is that their electronic structure relies solely on their geometry, making them a unique material in solid-state physics. Although pristine CNTs sheet resistance and transparencies are no match to ITO, their electrical conductivity can be improved by chemical doping treatments using strong acids or the entire electronic structure can be altered by modifying with certain chemicals. In addition, CNTs also have the upper hand of their compatibility in dry processes like arc-discharge, laser ablation and chemical vapor deposition, as well as wet processes. However, their high aspect ratio and strong van der Waals forces along the large surface areas of CNTs forms

aggregation, resulting in large bundles which makes it especially difficult preparing CNT dispersions and results in poor film quality.

Conductive polymers are also a promising material to replace ITO. Since the discovery of chemically doped acetylene, the organic electronic field so much so that photovoltaic technologies, organic light emitting diodes and field emmission transistors currently exist in our lives. Undoubtedly, PEDOT:PSS is the leading organic polymeric material, due to its affordability, processability , thermal stability and last but not least, its compatibility with cheap sol-gel coating techniques such as spin, spray, roll-to-roll etc. These four properties of PEDOT:PSS makes it extremely convinient for TCFs not only economically, but also its suitability in technical aspects for future flexible electronics. In fact, PEDOT:PSS is now considered as a standard chemical and can be found in many formulations up to 25 dispersions with different solid content, PEDOT:PSS ratios, viscosities and optoelectronic properties for any type of application ranging from OLEDs to PVs. Despite PEDOTs many great advantages, lifetime stability of PEDOT remains an open problem within TCF applications. When exposed to light and ambient air, PEDOT chemically degrades over time by oxidation, which decreases its conductivity. thus limits its use in outdoor applications.

Meanwhile, metal nanowires have also been attracting tremendous attention in publications based on their eletrocatalytic and optoelectronic properties in molecular and energy relating fields. Since then, many types of metal nanowires have been synthesized, such as silver nanowires (AgNWs), platinum nanowires (PtNWs), copper nanowires (CuNWs) and gold nanowires (AuNWs). Moreover, these synthesized nanowires (NWs) have been successfully fabricated in variety of cost-effective coating methods including mayer rod coating, brush painting, dip coating, spin coating and spray coating. Spesifically, AgNWs demonstrate the best performance, therefore are the most well-studied material within the metal nanowire TCFs. However, like any other TCF material, there are several drawbacks. Haze, which is defined as an optical phenomenon that occurs when light is scattered by the surface of the material, is the first contra point of AgNWs that comes to mind and is unfavorable because of its affect of appearance in quality. Moreover, AgNWs tend to reflect the light strongly, which means, touch panels and display screens made from AgNWs could make the content of the screen inperceptible to read. Surface roughness and adhesion are also

other challenges that AgNWs face with wet coating techniques resulting in limitations to their implementations into commercial technologies [28]–[30]. Another disadvantage is that even though AgNWs compatibility with cheap wet coating processes makes it a cheaper alternative compared to ITO, silver is more expensive than indium.

As evident from the discussions above, even though conductive polymers, carbon- and metal-based materials possess great unique advantages in TCF applications on their own; the shortcomings of these materials still remains an open problem in literature. To tackle this problem, TCFs could develop into composites that combine inorganic materials, nanomaterials, and organic materials in layers included in the device to overcome the drawbacks any one individual material to achieve higher performance through their integration.

2.1 Technical Aspects of TCFs

The essential requirements differ and depend on the spesific application of TCFs. To clarify, TCF that will be used as an electrode in a solar cell would require high conductivity and optical transmittance whereas in touch screen applications transparency is not considered one of the prerequisites. Therefore, it is important to introduce several important concepts before diving into properties of prospective materials of TCFs.

When economical and practical aspects are in consideration , a TCF material clearly must be non-toxic, colourless and cheap to produce. From a technical point of view, a material with high electrical conductivity (σ) must have high carrier concentration (η) of electrons (n) and holes (p) and/or high carrier mobility ($\mu_{n,p}$) which formulates as (2.1),

$$\sigma = e\eta\mu_{n,p} \tag{2.1}$$

where e is the elementary charge. Since electrons have smaller effective mass m^*, electrons are much more mobile than holes or ions. As a result, materials that are good conductors exhibit electrons as charge carriers. While an increase in carrier mobility and concentration should result in high electrical conductivity in a material, η is limited by the incident light absorbed by free carriers, electrons. The free carriers form a

plasma excitation or a 'plasmon' where the plasma frequency (ω_p) are calculated with the Classical Drude theory as equation (2.2),

$$\omega_p = \sqrt{\eta e^2 / m^* \varepsilon_r \varepsilon_0} \tag{2.2}$$

where m^* is the effective mass of the carriers (electrons) and $\varepsilon_r\varepsilon_0$ is the permittivity of the material. The energy of the plasmon (E_p) and its wavelenght (λ_p) are given in equations (2.3) and (2.4) respectively, where c is the speed of light.

$$E_p = c\omega_p \tag{2.3}$$

$$\lambda_p = 2\pi\hbar / \omega_p \tag{2.4}$$

Equation (2.1) and (2.2) formulated with respect to the carrier concentration, determines electrical and optical properties of TCF materials. Specifically, λ_p plays a key role in optical properties whereas carrier concentration and mobility are important for electrical properties. These formulas allow us to categorize TCFs into three individual groups: metal oxides or oxide semiconductors that exhibit high carrier concentrations ($\eta \sim 10^{21}$ cm^{-3}) and mobilities; metals that possess a very high carrier concentration ($\eta >> 10^{22}$ cm^{-3}) but medium mobilities; and carbon-based materials that possess relatively low carrier concentration and mobilities [1], [31].

Table 2.1 : Classification of TCF materials according to drude theory [32].

Categories	Material	Bulk resistivity (μΩcm)	Carrier concentration η (10^{21} cm^{-3})	Mobility μ ($cm^2V^{-1}s^{-1}$)
Metal oxides	ITO	> 100	< 3	≈20-100
	SnO_2	> 500	< 1	≈15-50
	ZnO	> 200	< 1	≈1-5
	TiO_2	> 500	< 4	≈10-70
Metals	Al	2.5	180	14
	Ag	1.5	58	72
	Cu	1.55	85	48
Carbon-based Materials	Polymers	> 700	< 10	< 1
	SWCNTs	> 150	3×10^{-4}	< 10
	Graphene	> 5	< 0.3	< 5000

As can be seen in Table 2.1, metals posses the highest conductivity among all three groups of TCF materials. However, the optical transparency of bulk metals are almost zero due to their absence of bandgap energies (E_g) and high electronic densities.

Meanwhile, metal oxides follow the Drude free-electron model very well and have excellent optoelectronic properties; for this reason these materials acclaimed wide popularity in the research field of TCFs to date. According to Coutts et al. (1998) study related to the Drude theory on TCOs, high carrier concentration corresponds to the classic brown appearance of metal oxide TCFs. Even though high carrier concentration means high conductivity according to equation 2.1, this leads to poor optical properties of the TCOs. Therefore, the best strategy to improve optical properties of TCF materials to decrease carrier concentration while increasing carrier mobility.

Carbonaceous materials like graphene and CNTs possess electronic structures unlike any other materials. While graphene is exceptional due to its high mobility at low carrier concentrations, CNTs, specifically single-walled carbon nanotubes, can be semiconductors with direct E_g, or metals absence of E_g, depending on the chirality of the nanotubes. The relation between chirality and electronic structure of nanotubes will be presented in Section 3.1.

2.1.1 Sheet resistance

Sheet resistance (R_{sh}) , is a measurement of a resistance of a thin film material having a resistivity (ρ) and a homogeneous thickness t which is defined as ,

$$R_{sh} = {}^{\rho}/_{t} \tag{2.5}$$

where (ρ) is a characteristic property of a material. The relationship between conductivity (σ) and sheet resistance (R_{sh}) is given as equation 2.6.

$$R_{sh} = {}^{1}/_{\sigma t} \tag{2.6}$$

2.1.2 Optical transparency

The optical transparency (T) of a thin film is another measure used to evaluate the performance of a TCF. It is formulated by the ratio of light intensity emitted through the thin film (I) to the intensity of the incident light (I_0),

$$T(\lambda)\ (\%) = {}^{I}/_{I_0}\ x\ 100 \tag{2.7}$$

where the incident intensity I_0 corresponds either to the electrode, which is the sum of both film and substrate intensities, or only to the film if the substrate is eliminated [1].

Optical transparency is described by the Beer-Lambert Law and the relationship is given as equation 2.8.

$$T(\lambda) = \exp(-at) \tag{2.8}$$

where t is the film thickness or the distance that light travels through the electrode and a is the absorption coefficient. The absorption coefficient is a function of the wavelength of incident light, which can also be defined as

$$a(\lambda) = {}^{4\pi k(\lambda)}/_{\lambda} \tag{2.9}$$

where k(λ) is defined as the extinction coefficient . Combining equations (2.6), (2.8) and (2.9) yields an inverse relation between transparency and sheet resistance as seen below.

$$R_{sh} = {}^{-4\pi k(\lambda)}\Big/_{\sigma\lambda\ln(T)} \tag{2.10}$$

The sheet resistance-tranmittance relationship in equation 2.10 is particularly important for TCFs based on carbon materials like graphene and CNTs and PEDOT:PSS. Since transparency and sheet resistance are inversely proportional to each other, the challenge with these materials is to increase the conductivity as much as possible while maintaining the transmittance in the visible range.

2.1.3 Figure of merit (FOM)

Optical transparency and sheet resistance of TCFs do not play a sufficient role in comparison of performances of studies done in literature. The relationship between transparency and resistance differ for various materials. Thus, TCF performances are typically compared and evaluated by using a figure of merit (FOM). The most common FOMs used in literature were defined by Fraser et al. [33] and Haacke et al. [34], for which the formulas are

$$F_{TC} = {}^{T}/_{R_{sh}} \tag{2.11}$$

$$\Phi_{FC} = {}^{T^x}/_{R_{sh}} \tag{2.12}$$

respectively, where T corresponds to optical transmittance in the visible range, R_{sh} is sheet resistance and x is an integer (~10).

3. PROSPECTIVE MATERIALS OF TCFs

Chapter 3 covers the electrical and optical properties of the TCF materials used in this thesis, namely SWCNTs, PEDOT:PSS and AgNWs, along with their respective structural properties.

3.1 Carbon Nanotubes (CNTs)

Since their discovery in 1991 by Iijima , CNTs have generated enormous attention within the TCF field. CNTs are classified into two primary types: single- or multi-walled carbon nanotubes (MWCNTs). The distinction between these forms is how the graphene sheet is constructed. While SWCNTs are formed by a single sheet of graphene rolled up to form a cylindrical 3D material, MWCNTs consist of multiple tubes of rolled graphene integrated inside each other. Figure 3.1 illustrates the concept of SWCNT formation and MWCNTs simplest form as double-walled carbon nanotubes (DWCNTs).

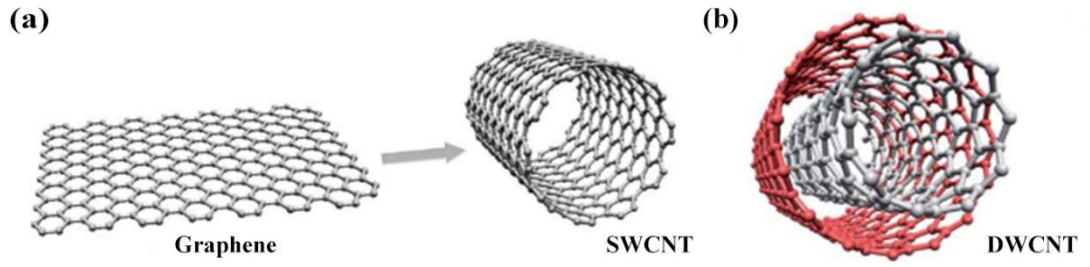

Figure 3.1 : Representation of SWCNTs (a) and (b) MWCNTs as DWCNTs.

MWCNTs, like SWCNTs, have remarkable mechanical characteristics and unique doping methods owing to their structure; nevertheless, CNTs main topic will focus only on SWCNTs.

3.1.1 Physical properties of SWCNTs

SWCNTs are similar in structure to graphene which is folded into a cylindrical shape of graphite sheets. The walls of the nanotubes are formed by carbon atoms of arranged in honeycomb patterns in the sp^2 hybrid network. The chemical sp^2 bonds give

SWCNTs extraordinary properties, such as mechanical strength and thermal stability. These properties make SWCNTs exceptionally promising for future flexible electronics.

The structure of SWCNTs is determined by the wrapping of the graphene sheet and is indicated by a chiral vector $\vec{C}$. The chiral vector results in a pair of integers which are shown as (n, m) and correspond to the graphene vectors of $\overrightarrow{\propto_1}$ and $\overrightarrow{\propto_2}$. The integers (n,m) have an impact on the diameter of the nanotube and are defined by chirality.

The following formula expresses the chirality.

$$\vec{C} = n\ \overrightarrow{\propto_1} + m\ \overrightarrow{\propto_2} \tag{3.1}$$

Where n and m are non-negative integers.

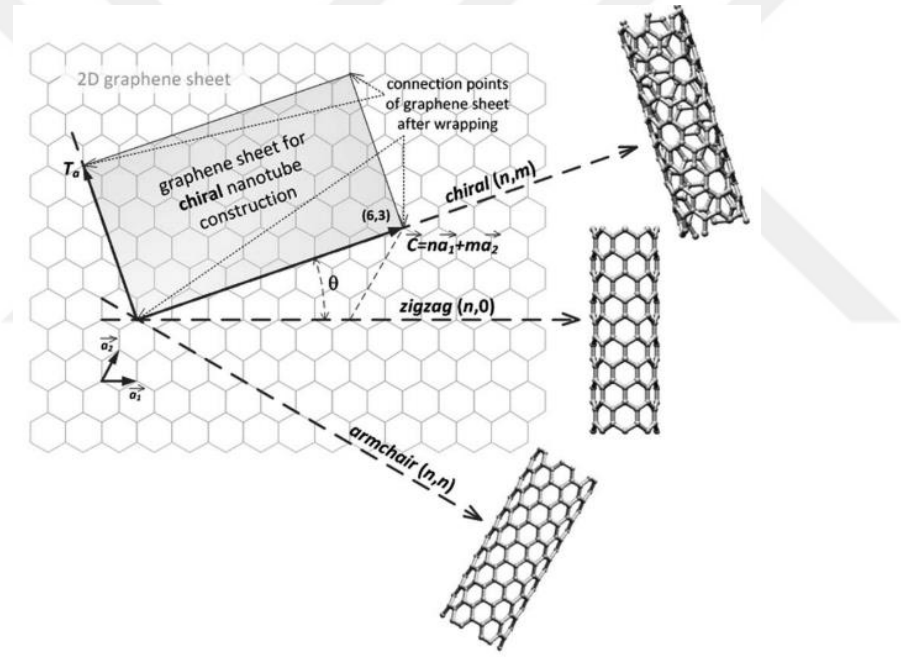

Figure 3.2 : The construction of SWCNT structures by chiral vector $\vec{C}$ [35].

The formation of SWNCTs are categorized into 2 common structures, namely zigzag and armchair [36] . As can be seen in Figure 3.2, the zigzag structure of SWCNTs will have a chiral angle θ of 0°, denoted by integers (n,0) where m equals to 0. When θ=30° the SWCNT structure is known as armchair and the integers are given as (n,n) where n equals to m . In addition to these configurations, an uncommon chiral construction of SWCNTs also exists. When nanotube chiral angle is between 0 -30° the structure is referred to as "chiral" , which is defined as n>m>0 [37] . The chirality of carbon nanotubes affects their electrical, optical and other characteristics.

Diameter of SWCNTs are given between 0.4- 4 nm [5]. Due to lack of research and SWCNTs possible tendency to collapse under atmospheric pressure, there are uncertainties of diameter measurements. However, the diameter is influenced by chirality, which also has a strong influence on the electronic structure of SWCNTs.

3.1.2 Electrical properties of SWCNTs

As previously stated, chirality plays a significant role in the electronic structure of SWCNTs. The integers (n,m) determine the SWCNTs' electronic characteristics to exhibit either semiconducting or metallic (s-SWCNT and m-SWCNT, respectively) behavior. The relationship between integers and the electronic behavior of SWCNTs defined as follows,

$$|n - m| = 3q \tag{3.2}$$

where q is an integer when SWCNTs are metallic. While the armchair configuration of SWCNTs is metallic, the zigzag and chiral constructions of SWCNTs possess semiconducting behavior. Moreover, equation 2.15 reveals that synthesized SWCNTs will statistically show semiconducting behavior in two-thirds, while metallic behavior in one-third. Depending on their Fermi energy levels (E_F), s-SWCNT can be hole or electron carriers as with typical semiconductors. In s-SWCNTs, the band gap energy and diameter are inversely proportional to each other. s-SWCNTs with larger diameter results in smaller band gap energies with higher charge carriers in room temperature [15].

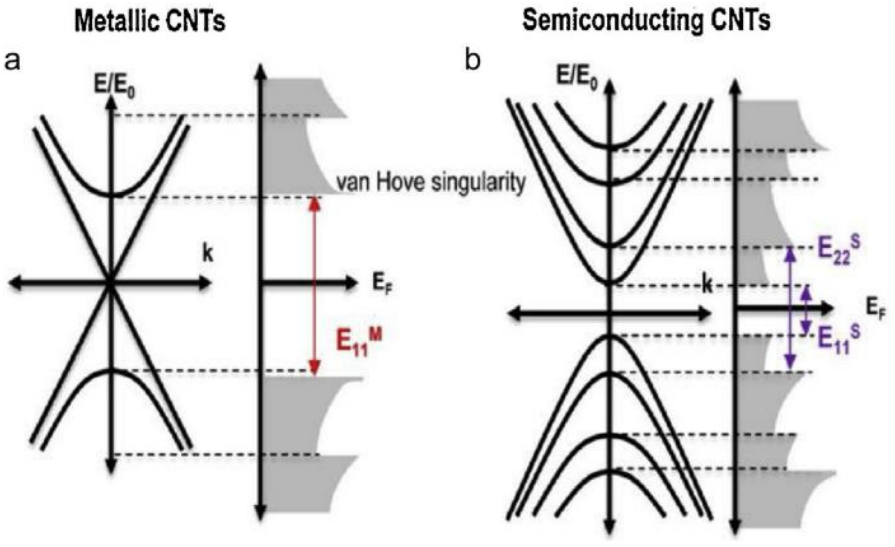

Figure 3.3 : Electronic band structures and density of states of (a) metallic and (b) semiconducting CNTs [38].

The electron transport mechanism in SWCNTs may be summarized as follows. The density of states (DOS) is defined as the number of available energy states for an electron to occupy. In bulk materials, the electron is not confined by the material, thus can move freely and has infinite number of energy states. However, in nanomaterials, the mobility of an electron is restricted to dimensions of one, two, or three with respect to the material. For instance, for 1D materials where the dimension is fixed to two directions, the electron can only move in one direction, resulting in a discrete and quantized DOS [39]. For this reason, SWCNTs exhibit unique distinctive levels of energy states known as van Hove singularities (vHs). The DOS of CNTs illustrated in Figure 3.3 shows the van Hove singularities denoted as E_{11}^{M} ,E_{11}^{S} and E_{22}^{S} of metallic and semiconducting nanotubes, respectively, where E_{11}^{M} is the lowest characteristic energy state for metallic and E_{11}^{S} is the first energy transition for s-SWCNTs [36].

3.1.3 Optical properties of SWCNTs

In addition to their chiralities, the respective van Hove singularities of m- and s-SWCNTs are highly associated with their optical characteristics. The absorption spectrum of an individual SWCNT can be measured using Uv-vis Spectroscopy by their electron transitions. Light absorption excites the electron from the valence band to the conduction band in s-SWCNTs, resulting in peaks. Since SWCNTs with metallic behavior have no band gaps, the absorption spectrum can be observed by their van Hove singularity in E_{11}^{M} transition. Figure 3.4 (a) depicts the absorption peaks plotted against the energies, corresponding to m- and s-SWCNTs.

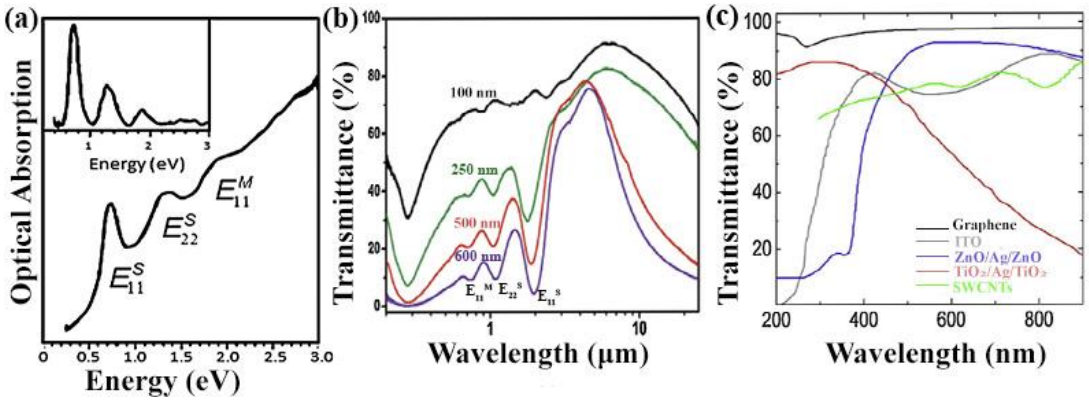

Figure 3.4 : (a) Optical absorption spectrum of a SWNT sample [40] and Transmittance spectra of (b) SWCNTs with varying thickness [41], (c) different TCFs [42].

SWCNTs also show a wide spectrum ranging from ultraviolet (UV) to infrared (IR) regions in contrast to TCOs in Figure 3.5 (c). However, absorption in electron transition E_{11}^{S} increases in Figure 3.4 (b) with increasing film thickness of s-SWCNTs, which explains the large proportion of optical transparency loss in SWCNT films [15]. According to Hecht et al., the remainder of the transmission loss is caused by reflection, which is quite insignificant (10 orders of magnitude smaller) in comparison to absorption. Light absorption at the wavelength of 500 nm is especially important for optical transparency measurements of SWCNT thin films [43].

3.1.4 Film fabrication of SWNCT-based TCFs

3.1.4.1 Purification and dispersion of SWCNTs

SWCNTs exhibit hydrphobic properties and strong van der Waals interactions around their tubular structure which has a significant effect on their dispersions. These forces interact with other individual SWCNTs to form large SWCNT aggregates or bundles, which makes it difficult to disperse in solvents. Numerous attempts have been made in the literature to develop effective methods for dispersing SWCNTs while preserving their performance [44]–[50]. Nevertheless, this still remains a challenge in SWCNTs to disperse without shortening or damaging the nanotubes. These methods can be summarized in 3 major categories, which have their unique advantage and disadvantages.

- Dispersing SWCNTs with high boiling point organic solvents or superacids [51]–[54] ,
- Dispersing SWCNTs in aqueous solutions using dispersing agents such as surfactants or other solubilization agents [49], [55]–[58],
- Dispersing SWCNTs with aqueous solutions by modifying the SWCNT surface with functional groups [59], [60].

High boiling point solvents such as N-methyl-pyrrolidone (NMP), polyethylene glycol (PEG), dimethylformamide (DMF), chloroform and dichlorobenzene (DCB) are widely used for dispersing unfunctionalized SWCNTs. However, since these organic solvents are carcinogenic, safer methods are preferred for the dispersion of SWCNTs. Additionally, organic solvents are claimed to be ineffective in dispersing SWCNTs at greater concentrations [15]. While studies have shown that superacids dissolve

SWCNTs directly at higher concentrations, this is not a desirable technique for commercial equipment owing to their severe corrosive properties. In this regard, solvents with lower boiling points that are capable to disperse SWCNTs at high concentrations will be a better alternative for large-scale manufacturing processes.

Dispersions in aqueous solutions assisted by anionic, cationic, zwitterionic and non-ionic surfactants are safer alternatives than organic solvents. Surfactants, or surface active agents, are employed to aid hydrophobic nanotubes in water solutions owing to their amphiphilic properties [61]. Most commonly utilized surfactants for water based dispersions are namely sodium dodecyl sulfate (SDS), sodium dodecyl benzene sulfonate (SDBS), Triton X-100 and sodium cholate (SC), which are proven to be successful in dispersing SWCNT with very high concentrations (~20 mg/ml) into individual nanotubes [2] . A major drawback to surfactant-assisted dispersions is that residual surfactants on SWCNT films significantly decrease the sheet resistance and therefore decrease the overall performance of the SWCNT TCFs due to their insulating properties. The insulating residual layer of the surfactant decreases tube-tube interaction and increases optical absorption within the SWCNT film. There are several methods to remove surfactants using post treatment methods such as chemically treating SWCNT films with strong acids like HNO_3 or high temperature annealing. Nonetheless, removal of surfactants is challenging and there is no consensus in literature regarding the adsorption mechanism of surfactants on the film surface [62].

Other dispersing agents including derivatives of cellulose, starches, polymers, DNA and polysaccharides are also widely used to aid SWCNTs solubilization in water [15]. Polymer-assisted dispersions are particularly advantageous for fine-tuning the viscosity of the SWCNT ink prior to spin coating and roll-to-roll manufacturing.

However, a limited amount of work has been published regarding this topic for TCF applications due to the challenges of removing the insulating polymer dispersant post production [2]. Another alternative to disperse SWCNTs is to modify the nanotube surface by introducing functional groups. The functional groups form covalent bonds with the nanotube walls, altering the nanotubes' surface properties by lowering their hydrophobicity toward other solvents. Improving SWCNTs solubility with functionalization can be established in two different methods: oxidating the nanotube tips and walls by the carboxyl, hydroxyl and carboxylate groups (Figure 3.5 (a)) or

inserting organic compounds such as arylalkylamines , long chained dodecyl aniline groups or aminopolymers which is illustrated in Figure 3.5 (b) [63]–[65].

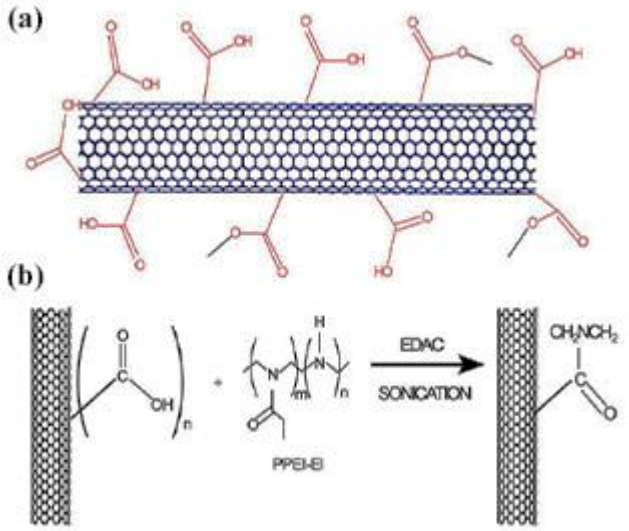

Figure 3.5 : A schematic representation of (a) organic groups, (b) an aminopolymer (PPEI-EI) attached to the nanotube surface [63].

Regardless of the dispersion method, high-energy mixing methods such as ultrasonic sonicators, homogenizers and ball milling are necessary to use for the separation of SWCNT aggregates. Ultrasonication is a commonly used technique to separate large bundles and decrease the diameter of the nanotube. However, excessive sonication results in structural defects and shortens nanotube length which is why sonication time and power are critical parameters to obtain ultra-long individual SWCNT dispersions.

3.1.4.2 Fabrication methods of SWCNT TCFs

There are several techniques for fabricating transparent conductive carbon nanotube films, including dry and wet processing methods. Due to its compatibility with current roll-to-roll coating processes, solution-based techniques are often utilized. Vacuum filtration [66], [67] , mayer rod [68]–[70], brush painting [71] , dip [72]–[74] spin [75], [76] and spray [16], [25], [60], [77]–[79] coating are all examples of solution-based processes. Each method has its own unique benefits and drawbacks.

Dip coating is one of the less complicated processes among other wet coating methods, where the substrate is dipped into the SWCNT ink and then dried . Viscosity plays an important role for dip coating, therefore choice of dispersant and concentration is key for high quality thin films of SWCNTs. While dip coating is a low-cost, easy, and

time-saving alternative compared to other techniques, significant drawbacks are that films are non-uniform and there is little to no control over film thickness.

Other variations of dip coating include brush painting and mayer rod method. Brush painting involves where a substrate is brush painted with the SWCNT ink, whereas in mayer rod method the ink is coated along the substrate with the help of a heated rod. Both of these techniques use shear force to coat the surface, and similar to dip coating, the downside of these methods is that the fabricated films are often inhomogeneous. The film performance of these films heavily depend on the surface tension and adhesion of the ink to the surface.

Vacuum filtration is another commonly used technique fabricating SWCNT films. The SWCNT ink is poured on a filter membrane where the CNTs form a network, then transferred by placing the filter membrane face down to the substrate. The transfer of the film to any substrate makes the vacuum filtration especially useful for flexible film fabrication. Additionally, this technique enables perfect control over the optical transparency of the SWCNT films by changing the concentration of the ink. Despite their excellent advantages , the film formation process is time consuming due to the filtration process, and the fabricated films exhibit high roughness and irregular morphologies.

Spin coating technique is employed by small volumes of SWCNT ink deposited onto the substrate to fabricate thin films. The spinning allows the ink to spread and dry on the substrate. However, the hydrophobic properties of SWCNT make it harder to achieve homogeneous films. To fabricate films with a specific thickness, multiple steps of the spin procedure must be employed, which also makes this method time consuming. With each spinning step, the SWCNT ink is wasted as a result of the rapid spinning of the plate.

Among all wet coating methods, spray coating is a desirable method because it is simple, repeatable, scalable and produces thin films of superior uniformity. Spray coating technique is conducted by spraying the SWCNT ink onto a heated substrate by either automatic spray coater or a simple air brush. Heating the substrate is key for spray coating technique, where the excess solvent is evaporated from the substrate during fabrication. This prevents the ink to form aggregates which is responsible of the distinctive “coffee stain” effect on the surface.

Owing to its straightforward approach to deposit materials on irregular surfaces and effortless control over the material thickness of the layers, extensive research has also been made towards SWCNT spray coating on flexible substrates [16], [80], [81]. In an article published in 2017, Lee and his colleagues fabricated flexible composite thin films by spray coating technique on polydimethylsiloxane (PDMS) substrate for flexible sensor applications using synthesized m-SWCNTs. They reported that the films optical transmittance was measured as 92% in the visible region with a visible dense SWCNT network structure [25] . Bu et al. developed flexible thin films by spray coating method on PDMS substrates using reduced graphene oxide (rGO) and SWCNTs. In their study, they emphasized that the optoelectronic properties of thin films fabricated with SWCNTs were superior to thin films with rGO. The sheet resistance of the SWCNT films decreased from 7800 Ω/sq to 670 Ω/sq when the nanotube concentration was increased from 0.01 mg/ml to 0.075 mg/ml. Additionally, they stated that the optical transmittance of the fabricated films with SWCNTs were higher than the rGO films, with a respective optical transmittance of approximately 60% in the visible region [16]. A study done by Gu et al. in 2019, SDBS surfactant assisted SWCNT dispersions were spray coated and chemical treatments were employed using HNO_3 and HCl at different concentrations to investigate the effects on the electrical conductivity of SWCNT films. It was determined that the nitric acid-treated films were highly effective in removing SDBS residues which significantly improved the electrical conductivity of the films. They found that the SWCNT film after nitric acid treatment had a transmittance of 85% in the visible region with a sheet resistance of 500 Ω/sq [82].

3.2 Conductive Polymers

The prominence of conductive polymers in the literature can be attributed to reasons such as being mechanically flexible, cheap, and processable. The attraction towards conductive polymers started with the discovery of electrically conductive polyacetylene in 1977. Shirakawa et al. proved that insulating materials can be electrically tuned by “doping mechanisms” which was the discovery of the conductive polyacetylene from insulating polyacetylene [83], [84]. Not only did their work had a significant influence on conductive polymers, but also on the area of nanomaterials, for which they were awarded the 2000 Nobel Prize in Chemistry. Since then, the most

successful discovery has been with PEDOT:PSS within conductive polymers. PEDOT:PSS is now considered as a standard chemical and can be found commercially under the name of Clevios^{TM} in many formulations up to 25 dispersions with different solid content, PEDOT:PSS ratios, viscosities and optoelectronic properties for any type of application ranging from OLEDs to PVs.

3.2.1 Synthesis and properties of PEDOT:PSS

PEDOT:PSS is the most popular and widely utilized p-type conjugated polymer among other polymeric materials, due to its adjustable electrical conductivity, chemical and mechanical characteristics, such as flexibility and stability, and transparency. Pristine PEDOT:PSS exhibits properties such as conductivity of 0.2-1 S/cm, Seeback coefficient of 12-16 μ/K and a FOM value of approximately 0.42 [85]. Due to their tuneable electrical conductivities with the help of different pre- and post-chemical doping treatments, the PEDOT:PSS structure and morphology were studied in literature in order to understand the doping mechanisms and enhance the overall conductivity.

The PEDOT:PSS polymer which was described as a core-shell structure in 1999, consists of a hydrophobic PEDOT backbone and hydrophilic PSS-rich chains, illustrated at Figure 3.6 [86]. While the PEDOT core is responsible for PEDOT: PSS's conductivity and acidity by releasing positively charged H^+ ions into water dispersions, PSS is an electrically insulating surfactant which aids the dispersion of PEDOT in water.

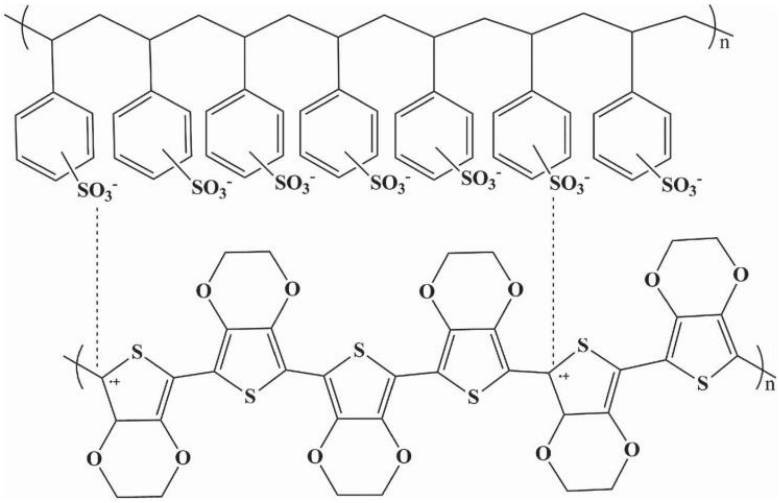

Figure 3.6 : Chemical structures of PEDOT:PSS [87].

PEDOT:PSS was first developed under the name Baytron™ but nowadays it is marketed under the name Clevios™. Many routes can be utilized for the synthesis of PEDOT:PSS. The first synthesis route was discovered by Bayer AG in 1998 where oxidizing agents were mixed with monomer, under the name EDOT in addition to a solvent. The synthesis route was discovered by Bayer AG in 1990. Elschner et al. reported the production of commercially available PEDOT:PSS as chemical oxidative polymerization [13] . In this synthesis, EDOT is added into the PSSH solution where the mixture is stirred continuously in a water bath at room temperature under nitrogen to enable the emulsification process. The addition of oxidants, namely sodium persulfate ($Na_2S_2O_8$) and iron(III) chloride ($FeCl_3$) jumpstarts the polymarization process of PEDOT:PSS, forming a complex. The synthesized complex is then diluted with double-distilled water. After the dilution the solution is mixed with an anion-exchange resin followed by filtering the resin, then repeating the same steps for a cation-exchange resin. In the final step, a desired solid content of PEDOT:PSS is added under a closed rotary evaporator flask under low pressure followed by dispersing the solution with a high-speed ultrasonic homojenizer to obtain mixtures with various pH, electrical conductivity and viscosity [88]–[90].

This synthesis enabled the commercialization of PEDOT:PSS solution in up to 25 different dispersions processable to produce thin films as thin as 100 nm and as thick as 1 μm [85], [91].

Other approaches for synthesizing PEDOT:PSS are continuously being researched by research organizations in order to produce more ordered morphologies and hence boost their mobility and electrical conductivity.

3.2.2 Electrical properties of PEDOT:PSS

The post-treatment methods of PEDOT:PSS alter the material's mobility, charge carrier concentration, and and structure, which also, as an end result, affects their transport mechanism. In the early studies of PEDOT:PSS, the electrical conductivity was measured to be approximately 0.1 – 10 S/cm. The improvement in conductivity by secondary doping was first established by MacDiarmid's research group in 1994 which is similar to the primary doping of EDOT to PEDOT taking place during oxidative polymerization [92]. This treatment procedure resulted in a several-orders-of-magnitude increase in conductivity and considerable modifications in the crystal

structure of PEDOT: PSS, as reported by several investigators. An example of this study was done by Kim et al. where different solvents were added into the commercial PEDOT: PSS solution, and addition of DMSO resulted in an increase from 0.8 to 80 S/cm in electrical conductivity. Another research group reported that the post treatment increased the conductivity of PEDOT:PSS due the modifications of chemical and structural characteristics [88], [93], [94]. They also stated that their XPS results showed a change in PEDOT to PSS ratio after post treatment which they associated with the removal of PSS chains from the grains and surface of the film. This was also reported subsequently by Crispin et al., who said that the solvent addition enhances the mobility between grains by increasing channels of charge transport. Interestingly, the core structure after post treatments significantly change with acids as well as organic solvents according to studies done by several researchers.

According to Ouyang et al.'s study, the post-treatments using ethylene glycol (EG) significantly altered the coil structure of PEDOT:PSS by showing in a linear/expanded structure after treatment. This phenomenon was also observed in another study using H_2SO_4 treatments [95], illustrated in Figure 3.7.

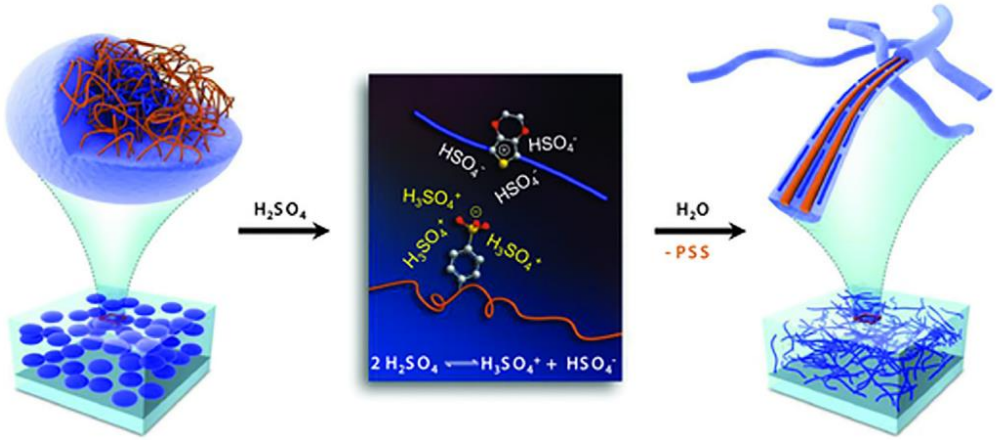

Figure 3.7 : A mechanism is proposed for the structural rearrangement of PEDOT:PSS after acid treatment [95].

3.3 Metal Nanowires

Metal nanowires are attributed as 1D materials which have a metal mono or polycrystalline structure. These materials exhibit extraordinary optoelectronic behavior and have received a great deal of attention in the literature due to their performance in a variety of TCF applications such as solar cells [30], touch screens [96], plasmonics [97], and heaters [98]. Up until now, researchers have synthesized

AgNWs, PtNWs, CuNWs AuNWs and as a result of these studies, it has become possible to produce nanowires with high purity with desired physical properties. In the field of metal nanowires, AgNWs are the most commonly investigated material owing to its high stability and straightforward synthesis compared to CuNWs. Furthermore, AgNW sheets can form highly conductive nanowire networks, making them superior to carbon nanotubes and a strong competitor to replace ITO. In light of these factors, this section will cover AgNWs unique optoelectronic properties.

3.3.1 Electronic properties of AgNWs

The early studies of metal nanowire TCFs optical transparency was under 80% with a high sheet resistance ranging from kΩ/sq-MΩ/sq, however, investigations in both theoretical and experimental areas have been carried out so extensively that metal nanowires now reveal an inspiring transparency of almost 91% and the sheet resistance as low as 50 Ω/sq. The conductivity of AgNWs is not only influenced by their metal characteristics, but also by their structure and other properties. The relationship between conductivity and geometry of AgNWs are still being investigated by researchers. Several groups have reported that the optoelectronic properties of AgNWs are heavily influenced by the nanowire structure such as length, diameter, and aspect ratio. For high electrical conductivity, the nanowires must be high in length and small in diameter with a high aspect ratio [28], [30], [96]–[100]. The density of the AgNW film is also a critical parameter for conductivity, however, junction resistance contributes to the sheet resistance increase in AgNWs due to the network forcing the electron to move across the junctions [96]. According to Hu et. al., junction resistance is reported to be as high as 1 GΩ, which is caused by impurities from synthesis that are insulating to the nanowires and poor networks [101]. Variety of techniques have been utilized to reduce the junction resistance, including welding using PEDOT:PSS [102] , heating [103], electrochemical annealing [104] , and pressing [105] .

In addition to junction resistance, adhesion and surface roughness have a decreasing effect to conductivity.

In summary, due to extraordinary optoelectrical properties that AgNWs possess, it is expected by many scientists that will replace ITO in the future. However, AgNWs are limited by their poor adhesion, high surface roughness and junction resistances that

still holds as challenges for commercial devices. Thus, more research must be done in order to overcome AgNWs drawbacks for commercialization.

3.3.2 Optical properties of AgNWs

Similar to their electrical properties, AgNWs optical properties are also affected by their geometry, density and nanowire structure. Andrés et al. studied effect of diameter and density of AgNWs on the optoelectronic properties, which is given in Figure 3.8.

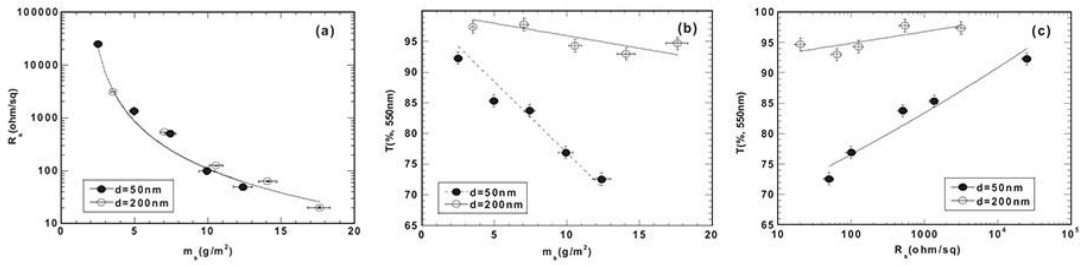

Figure 3.8 : (a) Sheet resistance and (b) optical transmittance (at 550 nm) for the AgNW films as function of silver content. (c) Direct relationship between sheet resistance and transmittance. [106]

As the diameter increases, AgNWs tend to scatter light and similar to SWCNTs and PEDOT:PSS, as the density (concentration of silver) on the surface increase, haze factor increases, which has a negative impact on optical transparency in TCFs.

4. EXPERIMENTAL

Chapter 4 covers the experimental setup and procedures to fabricate SWCNTs and the nanocomposites in great detail. The materials used in this thesis are listed in Section 4.1, and the experimental methods for fabricating SWCNT and nanocomposite films are given in 2 major sections, Sections 4.2 and 4.3, respectively.

4.1 Materials

Tuball™ single-walled carbon nanotubes (SWCNTs), PEDOT:PSS (Clevios PH1000,PH500, FET) were provided by OcSiAl and Heraeus, respectively. AgNWs were provided in powder form of 10 mg. Sulfuric acid (H_2SO_4, 95–98%) and nitric acid (HNO_3, 65%) were purchased from Merck. N-Methyl-2-pyrrolidone (NMP, 99.8%) and thionyl chloride ($SOCl_2$, %97) were obtained from Sigma Aldrich. As glass substrates, microscope slides (ISOLAB) with dimensions of 76x26x1mm were cut into 1.5x1.5 cm squares. The Millipore-Q system was used to prepare aqueous solutions using deionized water (DI).

4.2 Fabrication of Highly Conductive and Transparent SWCNT TCFs

4.2.1 Purification and dispersion of SWCNTs

The suspension of the SWCNTs used in the spray coating was prepared through the following purification and dispersion processes: 1 g of SWCNTs were treated with nitric acid solution with the concentration of 3M for 3h in order to improve the purity and remove metal catalysts. The purified product was rinsed several times with DI water until a pH of 7 was reached. The solution was subsequently filtered with a mixed cellulose ester (MCE, Whatman) filter followed by drying in an oven at 80°C. The purified SWCNT product was sonicated with NMP using an ultrasonic homogenizer (Bandelin) with an output power of 22.5 W for 90 minutes to obtain a stable dispersion. During sonication, the prepared SWCNT/NMP solution was adjusted inside an ice bath to avoid damage which might be caused by excessive heating. The dispersions

were then centrifuged to remove large bundles and other impurities, at 8000 rpm for 30 minutes, followed the collection 80% of the supernatant.

4.2.2 Substrate cleaning

Prior to the coating, glass slides with the dimensions of 1.5 cm x 1.5 cm were ultrasonically cleaned with ethanol, isopropyl alcohol and DI water, respectively, for 15 minutes. Next, the substrates were treated in an UV-ozon cleaner for further removal of organic substances, followed by drying in N_2 gas. Finally, in order to improve the adhesion and wettability of the surface, the substrates were treated with piranha solution (H_2SO_4/H_2O_2, 3:1) for approximately 7-9 minutes.

4.2.3 Fabrication of SWCNT films by Spray coating

Clean substrates were placed onto a hot plate the temperature of which was maintained at 200 °C. TCFs were prepared by adding different volumes (1 ml , 1.5 ml, 2 ml) of the supernatant of the SWCNT solutions which had been prepared with differing concentrations into the airbrush reservoir (Air Brush SATAgraph™ 3). The effect of volume was studied and the coatings varied with different thickness.

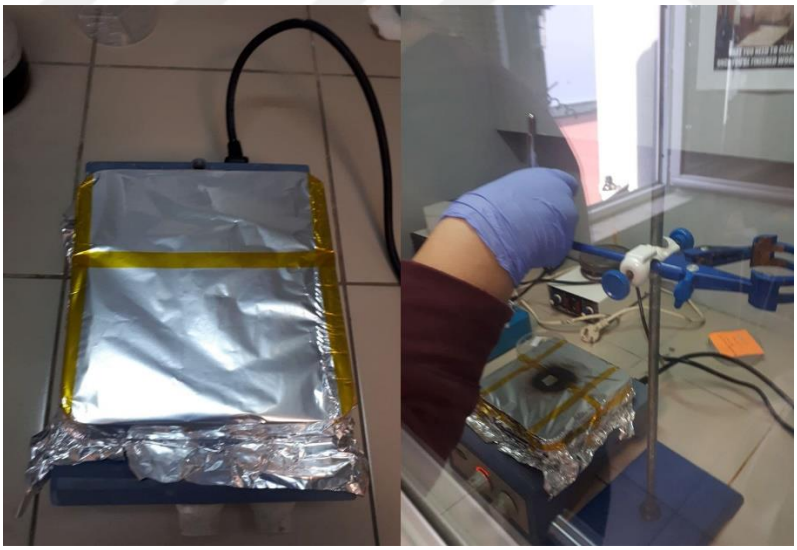

Figure 4.1 : Configuration of the spray coating system.

Throughout the fabrication, the temperature of the hot plate and the nozzle to substrate distance (10 mm) were kept constant and Kapton tape was used to secure each glass slide on the hot plate as seen in Figure 4.1 . Furthermore, the effects of carrier gas pressure (2, 3 and 4 bar) and SWCNT concentration (0.1, 0.2 and 0.3 mg/ml) on fabricated thin films were also investigated.

4.2.4 Post treatments of SWCNT films

To further reduce the sheet resistance, the spray deposited SWCNT thin films were chemically treated with HNO_3 and/or $SOCl_2$. Chemical treatments involving HNO_3 were conducted by using one of the following doping methods. Either

- immersing SWNCT thin film for 30 minutes, washing with DI water followed by drying at 80 °C for 10 minutes or
- applying drops onto the SWCNT thin film, washing with DI water then drying at 80 °C for 10 min.

To study the effectiveness of doping on the fabricated SWCNT thin films, the treatment time was also varied by 30 minutes to 1 hour with the optimized concentration and improvement method of HNO_3, HNO_3 and $SOCl_2$ treatments which were then combined to further study their effects on the electrical properties of the spray deposited SWCNT thin films. $SOCl_2$ treatments were carried out by immersion method for 30 mins followed by carefully drying under N_2 gas.

4.3 Fabrication of Nanocomposite TCFs

This section presents experimental methods of nanocomposite films. In order to benefit from SWCNT and PEDOT:PSS nanomaterials properties completely, the optimization of each material must be done correctly. Therefore, several factors were taken into account in formation of the experimental procedure.

The first step was to fabricate uniform and conductive SWCNT/PEDOT:PSS thin films, without reducing the optical transparency. Since PEDOT:PSS dispersions are acidic and have a distinctive dark blue colour, the film uniformity and transparency measures were taken into account to optimize the concentration of the PEDOT:PSS dispersions. Post treatment method was also conducted on the fabricated SWCNT SWCNT/PEDOT:PSS thin films by using DMSO.

Finally, AgNWs were added to the prepared SWCNT/NMP or PEDOT:PSS/DI dispersions and nanocomposites were produced with two different methods. The purpose of following these two different strategies was to investigate the compatibility of AgNWs in SWCNT and PEDOT:PSS ink and compare the performance of the fabricated nanocomposites. Since AgNWs have a tendency to have adhesion , contact

resistance and surface roughness problems, a second approach to fabricate nanocomposites were necessary to this thesis.

4.3.1 Fabrication of SWCNT/PEDOT:PSS films

PEDOT:PSS formulation was first filtered with a PVDF filter with a membrane thickness of 0.45 μm. Then, the solution was diluted with DI water to obtain 1:1 volumetric ratio. The test tube was placed onto a magnetic stirrer and kept at a constant rpm for 20 minutes. The prepared PEDOT:PSS dispersion (PH 1000, PH 500, Clevios FET) was spin coated (1 ml) on the SWCNT thin film in 3 steps (1500 rpm 15 sn as the 1st step, 2000 rpm 50 sn as the 2nd and 3000 rpm 1 sn as the final step).

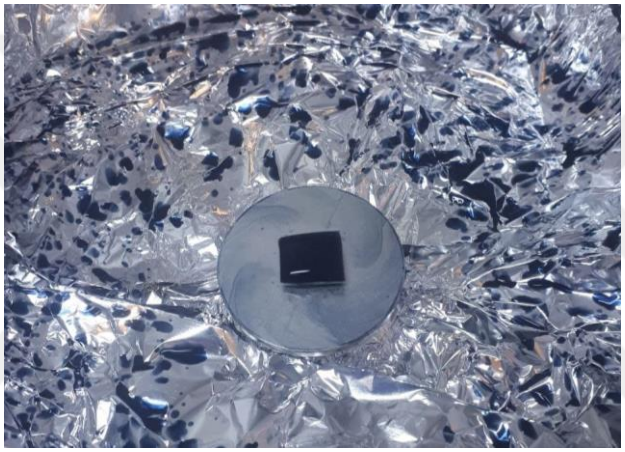

Figure 4.2 : Presentation of an evenly distributed PEDOT:PSS solution on the SWCNT thin film.

To obtain a homogeneous PEDOT:PSS layer, 1 ml of the solution was deposited onto the SWNCT film in 500 μL volume in 2 layers. The second PEDOT:PSS layer was coated while the film was still wet from the first layer. The solution was spread as evenly and carefully as possible. For the last step, the fabricated thin film was placed on a hot plate to anneal at 120 °C for 15 min in ambient atmosphere.

4.3.2 Post treatments of SWCNT/PEDOT:PSS TCFs

It is well known that in PEDOT:PSS thin films the addition of chemical solvents such as DMSO, sorbitol and EG as a post treatment method significantly increases their conductivity. Thus, in order to increase the conductivity without decreasing the transparency, the fabricated SWCNT/PEDOT:PSS thin films (w/PH 500, Clevios FET) were subjected to DMSO treatments. After the annealing step, the thin films were

placed onto the spin coater once again and treated with 50 μL of DMSO. Then, the films were put back on the heater (120 °C) to dry in ambient atmosphere.

4.3.3 Fabrication of SWCNT/PEDOT:PSS-AgNW TCFs

0.05 mg of AgNW powder was added to the PEDOT:PSS ink. The solution was placed onto a magnetic stirrer with a fixed rpm to disperse for 30 minutes. Then, the dispersed solution was spin coated onto the SWCNT film to form a nanocomposite. The spin coating procedure were kept the same and the films were annealed for 20 mins at 120 °C.

4.3.4 Fabrication of SWCNT-AgNW/PEDOT:PSS TCFs

As described in Section 4.2.1, the procedure of the SWCNT/NMP solution (0.1 mg/ml) was kept the same. After the centrifugation step, 0.05 mg of AgNWs were added into the SWCNT ink. The mixture was sonicated with an ultrasonic homogenizer with an output power of 22.5 W for 20 minutes to obtain a homogenous SWCNT/AgNW solution. After the sonication, the SWCNT/AgNW ink was deposited onto clean substrates which was placed onto a hot plate. The temperature and the nozzle distance was kept the same with the previous SWCNT thin film preparation. The spray gun pressure and spray volume was adjusted to 2 bar and 1.5 ml respectively. The sheet resistance and optical transparency values were measured, then the optimized PEDOT:PSS solution was spin coated as a final layer to obtain SWCNT/AgNW/PEDOT:PSS thin films. The films were then annealed at 120 °C for 20 minutes.

5. RESULTS AND DISCUSSION

Chapter 5 represents the results of SWCNT- and nanocomposite TCFs which is given in 2 major sections, namely Sections 5.1 and 5.2. Section 5.1 covers the evaluation of SWCNT-TCFs while Section 5.2 discusses nanocomposite TCF results.

5.1 Evaluation of SWNCT-TCFs

SWCNTs dispersed in organic solvent (NMP) were used in thin film preparation with the spray coating technique. SWCNT/NMP solutions at different concentrations (0.1, 0.2, 0.3 mg/ml) were prepared for the spray process at different carrier gas pressures (2, 3 and 4 bar) and volumes (1, 1.5 and 2 ml) to obtain highly conductive transparent thin films. After determining the sheet resistance and optical transmittance, the fabricated thin films were treated with 14.3 M HNO_3 using a variety of treatment methods such as immersing or applying drops to the film to minimize the damaging effect on the film. With the optimized HNO_3 method, the fabricated films were also treated by incorporating $SOCl_2$ (97%) into the post treatment regime in order to study the effect of p-doping and increase their conductivity.

5.1.1 TG and DTG analyses of SWCNT powder

Structural properties such as nanotube diameter, chemical stability and thermal resistance are important in the use of SWCNTs as a TCF material. The charge transport of SWCNTs are influenced by factors such as doping level and purity of the SWCNT product. Among these factors, purity plays an important role in resistance of films due to the defects in sp^3 bonds and amorphous carbon material leading to charge scattering and resistance in SWCNT thin films [37]. In this context, the pristine and purified Tuball SWCNTs were analyzed by TG and DTG analyses. In Figure 5.1 TG and DTG analyses results revealed that commercial Tuball SWCNTs consisted of 16.94% metal content and high burning temperature of 615.76 °C from the sharp peak. After the purification step, which was done by using 3M HNO_3, the metal content showed a decrease of 4 %, resulting in high purity SWCNT with less metal impurity content.

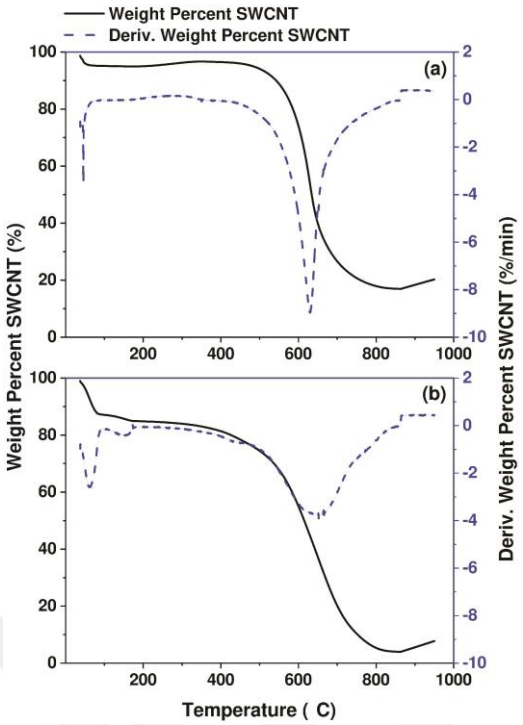

Figure 5.1 : TG and DTG analysis on (a) pristine and (b) purified Tuball SWCNTs.

5.1.2 Effect of surface modification on substrates

The wettability of the surface in solution-based coatings is an important factor to obtain good uniformity of SWCNT thin films. The optical transparency and sheet resistance parameters of thin films have a strong relationship with the substrate cleanliness and adhesion with the solution. As the contact angle increases, the solution becomes harder to deposit onto the glass substrate and results in poor film quality due to the substrate's hydrophobicity. Using smaller angles, production is easier and better quality films can be produced. Therefore, cleaned glass substrates were post treated with piranha solution (H_2SO_4/H_2O_2, 3:1) to reduce organic impurities and improve the wettability of the glass surface.

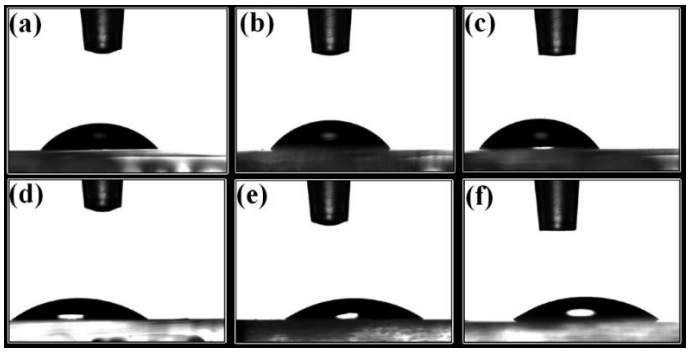

Figure 5.2 : Contact angle images of (a),(b),(c) untreated and (d),(e),(f) piranha treated glass substrate.

Water contact angles (CA) of untreated and piranha treated glass had averages of 53.04° and 35.23°, respectively. As can be seen in Figure 2, piranha treatment successfully reduced the contact angle of the water droplet by the possible addition of functional groups, resulting in a decrease in the CA mean. A more significant decrease in the contact angle could be attained by elongating the treatment time of piranha solution, as studied in literature [107]. However, unlike other wet coating methods such as meyer rod, spin, dip and LBL coating techniques, it is not a compulsory requirement to have low surface tension and contact angle values to obtain high quality thin films in spray coating method [43].

5.1.3 Effect of carrier gas pressure on SWCNT TCFs

The effect of carrier gas pressure is one of several important parameters which influences the film quality in the spray coating technique. Working at the appropriate pressure during coating directly affects the homogeneity which in turn leads to high sheet resistance due to agglomeration on the surface and/or low optical transparency of the fabricated thin film. Therefore, the carrier gas pressure effects on the fabricated thin films at air pressure of 2, 3 and 4 bar were investigated. Spray coating was conducted by using a concentration of 0.3 mg/ml. Optical transmittance of the produced films were measured and sheet resistance values were taken on 6 occasions and the averages were calculated.

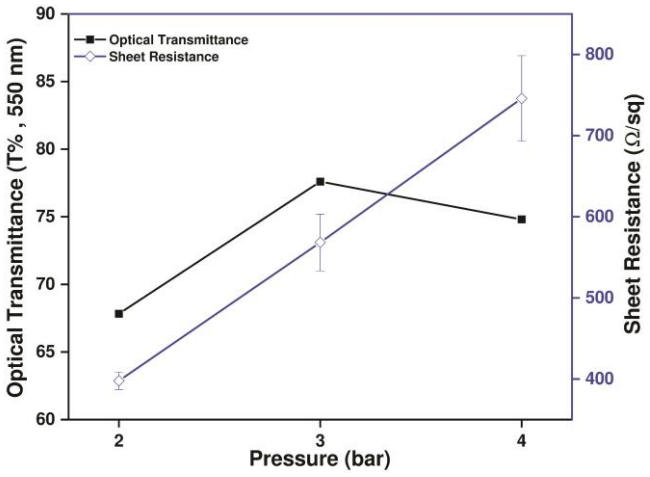

Figure 5.3 : Sheet resistance vs. optical transmittance plot for the SWCNT thin films prepared with different carrier gas pressures.

Figure 5.3 shows that the sheet resistances of the films fabricated at 2, 3 and 4 bar working pressure were determined to be 400, 570 and 750 Ω/sq, respectively. These

results reveal that the sheet resistance and standard error of the films decrease as the gas pressure decreases. Moreover, the plot also suggests that the optoelectrical properties of the SWCNT network formation increase with decreasing pressure. As the carrier gas pressure increased, the solution atomized onto the substrate did not thoroughly evaporate during deposition, which resulted in the dewetting phenomenon on the substrate. The accumulation of the SWCNTs was pushed by the high flow rate of atomized SWCNT solution towards the edges of the glass substrate, resulting in a disrupted, inhomogeneous structure. Although the concentration of the solution and spray coated volume were kept constant for all of the fabricated thin films, this observation explains the extreme change in sheet resistance of the films prepared under identical conditions. The decrease in standard error and sheet resistance could also be the result of the less small sized droplets depositing onto the film substrate as the carrier gas pressure decreases, thus resulting in better film quality and uniformity. As part of these results, the optimum working pressure for spray coating was chosen to be 2 bar.

5.1.4 Effect of SWCNT concentration on SWCNT TCFs

SWCNTs contain strong van der Waals forces in their structures. These forces cause SWCNTs to form bundles and agglomerate during dispersion, as a result, the poor dispersion of the mixture impairs the homogeneity of the produced films. Therefore, preparing SWCNT/NMP solutions at the appropriate concentration is of great importance in the fabrication of SWCNT thin films. Additionally, by varying the concentration of the SWCNT thin films, the optoelectronic properties of the films can be individually adjusted.

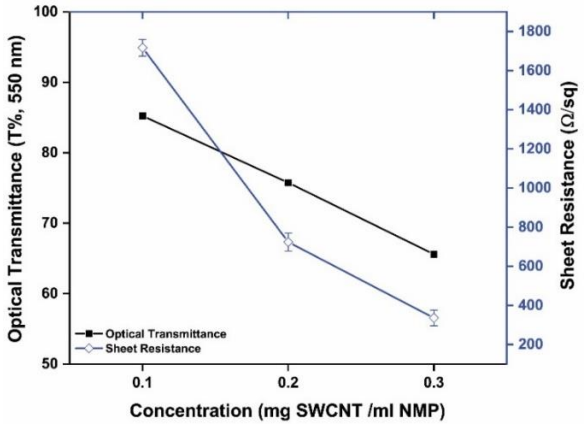

Figure 5.4 : Sheet resistance vs. optical transmittance plot for the SWCNT thin films prepared with different SWCNT concentrations.

Using 1 ml of the dispersed solution from each concentration, films were fabricated by spray coating on a piranha-treated clean glass. The sheet resistance and optical transmittance of the fabricated films are given in Figure 5.4.

Figure 5.4 shows that as the SWCNT concentration increases, sheet resistance and optical transmittance decrease. The sheet resistance of the prepared film at a concentration of 0.1 mg/ml is 1710 Ω /sq, while the thin film resistance obtained at concentrations of 0.2 and 0.3 mg/ml is 900 and 340 Ω/sq, respectively. The optical transparency of the films prepared at 0.1, 0.2 and 0.3 mg/ml SWCNT concentrations were determined as 85%, 83% and 65.5%, respectively. While the electrical conductivity at the concentration of 0.3 mg/ml is found to be best among the other prepared thin films, the optical transmittance value is extremely low for many TCF applications. Furthermore, it should be noted that a good dispersion could not be attained due to the agglomeration of SWCNTs. Even after the centrifugation step, a large amount of suspended particles was still observed within the suspension. Therefore, 0.1 and 0.2 mg/ml were chosen as the most suitable concentrations. Optoelectronic properties of the films can also be tuned by the volume sprayed onto the film during coating due to varying thickness.

5.1.5 Effect of spray coated volume on SWCNT TCFs

SWCNT solutions prepared at concentrations of 0.1 mg/ml and 0.2 mg/ml were coated on a glass surface in different spray volumes (1, 1.5 and 2 ml) and results of the obtained films are given in Figure 5. The optoelectronic properties of the spray-coated films vary using different volumes which is associated with film thickness. In Figure 5, the sharp change in the sheet resistance and optical transmittance of thin films prepared with both SWCNT concentrations with different solution volumes can be clearly seen. Figure 5.5 (a) shows the film prepared using 1 ml solution volume and 0.2 mg/ml SWCNT concentration was determined to have a sheet resistance of 720 Ω/sq while the films prepared with 1.5 and 2 ml solution volumes showed a significant decrease of 288 and 189 Ω/sq, respectively. However, when the volume of coating increased, the optical transmittance of the films decreased from 75% to 53% for 1.5 and 46% for 2 ml. A similar situation is observed in films prepared using 0.1 mg/ml SWCNT concentration shown in Figure 5.5 (b). For the films coated with 1, 1.5 and 2

ml volume, the sheet resistances were resulted in as 1720, 500 and 320 Ω/sq while the transmittance values were determined as 85% , 76% and 72%, respectively.

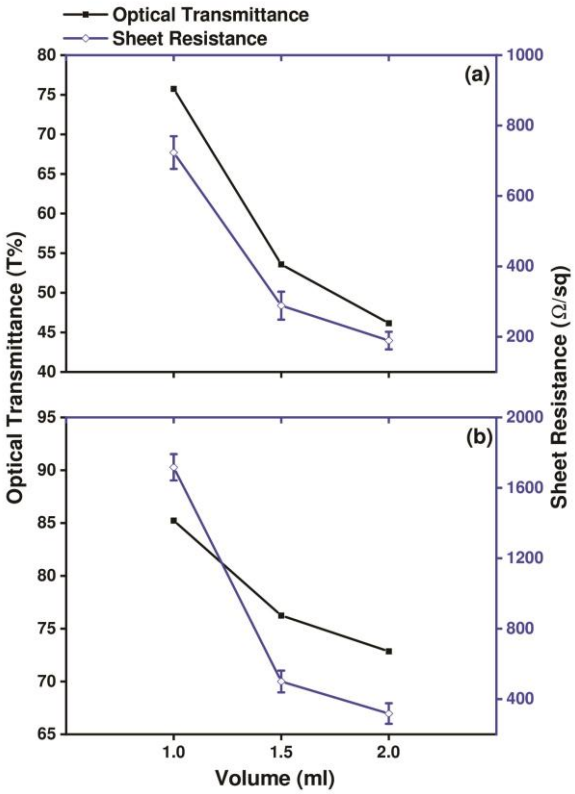

Figure 5.5 : Sheet resistance vs. optical transmittance plot for the SWCNT thin films prepared with different volumes at (a) 0.2 mg/ml and (b) 0.1 mg/ml concentration.

This implies that as the concentration and spray coated volume decrease, both sheet resistance and transmittance become more suitable. Further proof can be seen in SEM and AFM results of the 0.1 mg/ml SWCNT thin films.

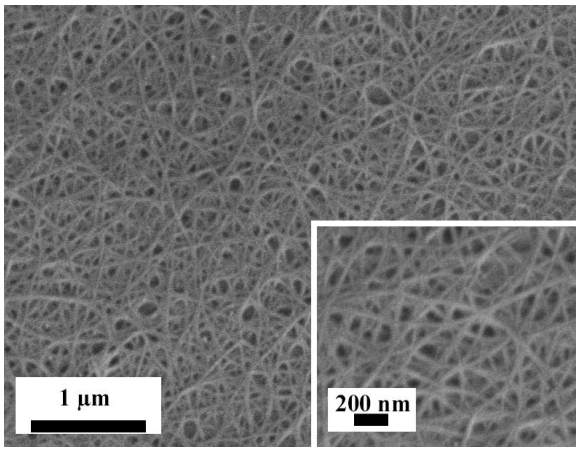

Figure 5.6 : SEM images of 0.1 mg/ml SWCNT spray coated film.

Figure 5.6 shows 0.1 mg/ml SWCNT of 2 ml spray coated film's SEM images. The morphology of both images show densely packed SWCNT networks which is expected as they demonstrated low sheet resistance values without any chemical post treatments. The formed SWCNT tubes are seen to be in very close contact with each other, therefore interpreted as having fewer voids occurring on the surface of the thin films.

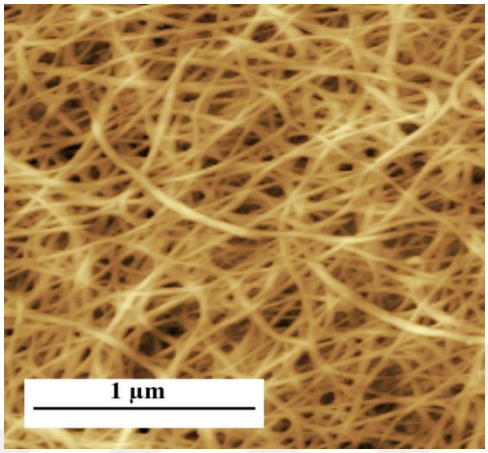

Figure 5.7 : AFM image of spray coated SWCNT thin film (0.1 mg/ml conc. with R_s and T % values of 289 Ω/sq and 83 % at 550 nm respectively).

Furthermore, the atomic force microscopy (AFM) image of spray coated SWCNT film can be seen in Figure 5.7 The 1.5 ml spray coated film had an average roughness (R_a) of 12.6 and a root mean square (R_{ms}) value of 15.6. The roughness values are consistent with other studies found in literature (R_a and R_{ms}) using spray coating [108] and the AFM images were found to be highly uniform with a low standard error and dense SWCNT network.

5.1.6 Post treatment effects on SWCNT TCFs with HNO_3 and $SOCl_2$

Nitric acid doping serves as one of the most effective dopants in literature. During HNO_3 treatment, the SWCNT TCFs become chemically doped by the addition of electron holes onto the surface, which results in p-doping of the thin film [109], [110].

As a result of the synergistic effect of acidity and oxidizability, a significant decrease in sheet resistance occurs in SWCNT thin films. However, HNO_3 solutions may damage the SWCNT TCFs, and due to its reactivity may cause the film to tear apart and peel off during post treatment. The lack of robustness in post treated films will limit the fabricated SWNCT's film potential in many applications and result in a decrease in the device lifespan [111]. To overcome the issues of the adhesion of the

surface of SWCNTs, chemical treatments involving HNO_3 were conducted by using various doping methods.

The investigation of different HNO_3 treatment techniques were conducted by applying immersion and drop methods to two separate SWCNT thin films, with R_s values of 318 and 357 Ω/sq, respectively. After treatment the R_s values were measured as 147 Ω/sq for immersion and 146 Ω/sq for drop method. The results indicated that there is a slightly greater decrease in sheet resistance using the drop method in comparison to the immersion method.

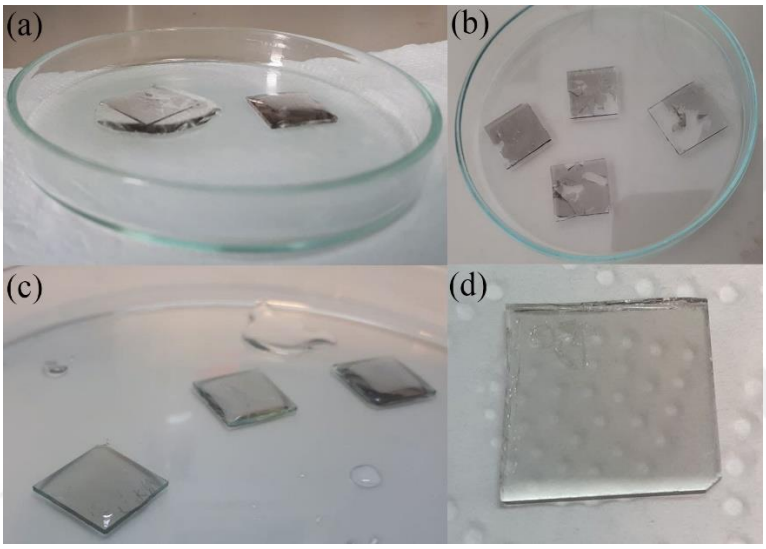

Figure 5.8 : HNO_3 treatments on SWCNT films with (a),(b) immersion method and (c),(d) drop method.

Furthermore, immersing the fabricated thin film in strong HNO_3 solution caused extreme damage to the film during post treatment, while the drop method retained the doping effect along with keeping the SWCNT film intact and undamaged.

Prior to the attainment of the results presented above, the treatment time was also studied. Regarding samples between 1-4, the concentration (14.3 M) and treatment method for HNO_3 were kept the same when the treatment time varied (30 and 60 min). After placing both samples inside a clean petri dish, HNO_3 drops were applied to cover the surface of the thin film. 30 minutes later sample 1 and 3 were taken out, washed with DI water and dried at 80 °C in an oven. Sample 2 and 4 were kept for 60 min, the same procedure was repeated as mentioned above, and the results were given in Table 5.1. Figure 5.8 (c) and (d) illustrates that the film quality was intact and no peel off occurred during post treatment. This slight difference between samples is an indicator that as the treatment time increased, HNO_3 continued to chemically oxidize the surface

of the thin films by the attachments of functional groups. The decrease in sheet resistance could also be a result of the decrease in film thickness where HNO_3 is known to be an effective treatment to remove NMP from the film surface [109].

Table 5.1 : The sheet resistance values of post treated films prepared with different spray coated volumes.

Sample No	Concentration (mg/ml)	Spray coated volume (ml)	Treatment time (min)	Chemical Treatment	R_s (as prepared) (Ω/sq)	R_s (post treated) (Ω/sq)
1	0.1	1.5	30	HNO_3	332	98
2	0.1	1.5	60	HNO_3	330	103
3	0.1	2.0	30	HNO_3	440	89
4	0.1	2.0	60	HNO_3	557	87
5	0.1	1.5	30	HNO and $SOCl_2$	329	123
6	0.1	1.5	60	HNO_3 and $SOCl_2$	330	129
7	0.1	2.0	30	HNO_3 and $SOCl_2$	447	80
8	0.1	2.0	60	$HNO_3$and $SOCl_2$	580	149

Raman spectra were also carried out for treated and untreated SWCNT TCFs to characterize the effect of HNO_3 with a 532 nm excitation laser wavelength (2.33 eV). The spectra is given in Figure 5.9 and shown in 3 panels as (a), (b) and (c): 100-250, 1300-1800 and 2500-2900 cm^{-1} where the peak changes occur for radial breathing mode (RBM), D, G and G' band respectively. At a laser excitation wavelength of 532 nm, the as prepared SWCNTs were excited as can be observed from the RBM peak which occurred at low frequencies of the spectra (100-250 cm^{-1}) at Figure 5.9 (a).

The D peak at 1345.16 cm^{-1} reveals defects and impurities within the sample whereas the sharp G band observed at 1594.6 cm^{-1} is an essential characteristic peak for SWCNTs correlated with carbon atom vibrations within the graphitic plane. The intensity ratio of the D band to G band I_D/I_G ratio reveals the degree of disorder and defect formation on the sidewalls of the given SWCNT sample. The as prepared and nitric acid treated SWCNT TCFs ratios were calculated as 0.025 and 0.030, respectively. Our results were lower than studies done in literature [49], [82], [112] and can be attributed to the purification of commercial Tuball SWCNTs (75%) done by 3 M HNO_3, which was disclosed above (see Section 4.2.1). Extremely low D peaks observed at 1345 cm^{-1} (as prepared) and 1377 cm^{-1} (HNO_3 treated) shown in Figure 5.9 (b) are also indicators which reveal that high purity SWCNT powder (96%) was obtained after the acid reflux treatment. It should also be noted that the purification

step may also be a dominant factor of a significant difference in sheet resistance of the thin films.

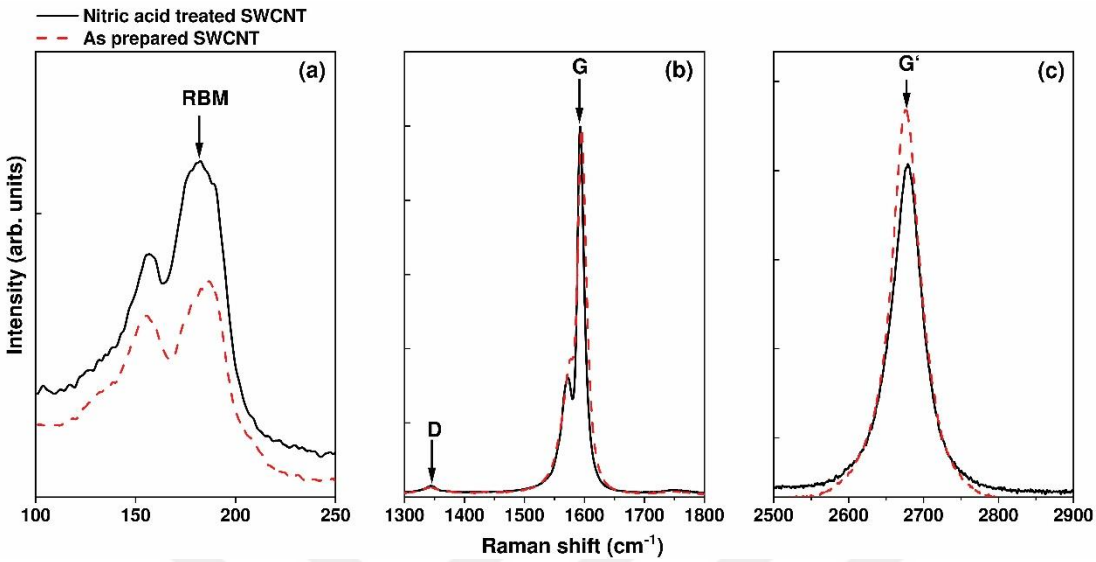

Figure 5.9 : Raman spectra (at 532 nm) of untreated and HNO_3 treated SWCNT thin films.

The increase in I_D/I_G values reveals that the structure of the surface has been changed by the HNO_3 treatment due the introduction of p-type carboxylic acid groups into the C–C sp^2 bonds of the SWCNTs. In addition, a slight blue shift of 1.1 cm^{-1} in the G band occurred and RBM intensity was severely suppressed for nitric acid treated SWCNT TCFs. The raman spectra reveals that HNO_3 treatment was effective promoting charge transfer and the peak shift suggests the possibility of functionalization of SWCNT, resulting in p-doping of the thin film. Large shift in G band and high intensity ratio difference in comparison to the study employed here could be due to purification on SWCNT prior to coating. For this reason, the results presented here are considered to be in good correlation with other studies done in literature [49], [113], [114].

Another commonly used p-type dopant for SWCNT-TCFs in literature is $SOCl_2$. P type doping using $SOCl_2$ results in the nucleophilic substitution of carboxylic acid groups on the sidewalls and more electronegative acyl chlorides on tips of the SWNTs [115]. A study showed that $SOCl_2$ doping is an effective method to increase conductivity in both SWCNT and SWCNT composite thin films by their exceptional electron withdrawing ability [116], [117]. Table 5.1 also shows the SWCNT thin film parameters of as prepared and treated TCFs with HNO_3 and $SOCl_2$ *p*- dopants (sample

numbers between 5-8). The treatment time was varied (30 mins and 60 mins) for HNO_3 treatment then combined with $SOCl_2$ to study further improve the conductivity.

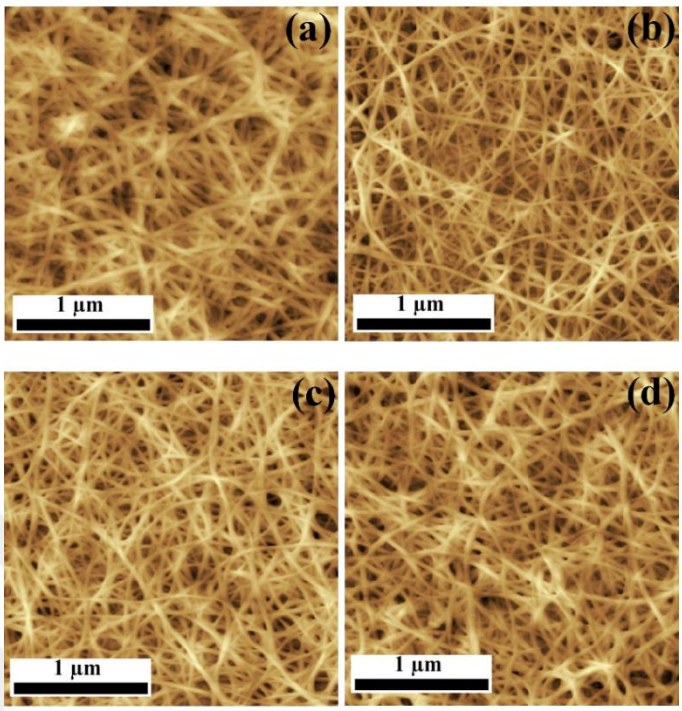

Figure 5.10 : AFM Images of HNO_3 and $HNO_3/SOCl_2$ films: (a) 30 min HNO_3, (b) 60 min HNO_3 , (c) 30 min HNO_3/30 min $SOCl_2$ and (d) 60 min HNO_3/30 min $SOCl_2$.

The surface morphologies of chemically treated SWCNT films are compared in Figure 5.10. Several bright peaks are observed in the structure of the SWCNT thin film. Images of the CNT networks captured by AFM were found to be highly uniform with all post treated samples, which is crucial for achieving a uniform performance in any application areas of TCFs. The roughness of the HNO_3 treated films showed a decrease in R_a of 10 nm and R_p from 50 to approximately 43 nm with both 30 and 60 minutes of treatment. However, with the incorporation of $SOCl_2$ into the chemical treatment, the R_a slightly increased to 12 nm.

In this study Haacke's FOM formula was used to compare the post treated SWCNT thin film performances and are shown in Table 5.2 . The FOM values were calculated from Table 5.1 using the sheet resistance values after treatment with their transparencies from Table 5.2 . The post treated SWCNT thin films demonstrated excellent electrical conductivity in the company of both HNO_3 and $HNO_3/SOCl_2$, with FOM values between 8.2×10^{-4} – 2.0×10^{-3}. The FOM values resulting from this study show that electrical and optical properties are heavily dependent on proper optimization of the fabrication and post treatment techniques.

Table 5.2 : FOM calculations of post treated SWCNT thin films of our work and previous studies.

Sample No	R_s (Ω/sq)	T (%) at 550 nm	Figure of Merit (FOM)	Fabrication Method
1	98	83	1.6×10^{-3}	Our work
2	103	85	2.0×10^{-3}	
3	89	75	6.0×10^{-4}	
4	87	80	1.2×10^{-3}	
5	123	83	1.3×10^{-3}	
6	129	82	1.0×10^{-3}	
7	80	75	7.0×10^{-4}	
8	149	81	8.2×10^{-4}	
Ref. 16	57	65	2.4×10^{-4}	Spray coating
	68	70	4.2×10^{-4}	
Ref. 17	59	71	5.5×10^{-4}	Spin coating
Ref. 19	125	87	2.0×10^{-3}	Spray coating
Ref. 23	472	85	2.1×10^{-4}	Spray coating
	956	85	4.2×10^{-4}	
Ref. 25	670	60	9.0×10^{-6}	Spray coating
Ref. 45	100	70	2.8×10^{-4}	Rod coating
	300	90	1.1×10^{-3}	

In Table 5.2 , this work outperforms compared to other studies done by using SWCNTs [16], [75], [79], [80], [118], [119] with spin and rod coating methods. This could be explained by difficulties in uniformity and achieving dense CNT networks. Lastly, the high FOM values calculated from our fabricated films are similar to each other, which shows the consistency of this work. The constant profile of these values point to another clear indicator that highly dense CNT networks were formed by the optimization of the experimental set up and post treatment methods.

5.2 Evaluation of the Fabricated Nanocomposite TCFs

5.2.1 Evaluation of the fabricated SWCNT/PEDOT:PSS TCFs

5.2.1.1 Effect of PEDOT:PSS/ DI water Concentration

The properties of commercially available PEDOT:PSS/Water dispersions are given in Table 5.3 . The dispersions need to be adjusted in order to fabricate uniform films. Particularly, the viscosity of PEDOT:PSS dispersions have significant effect in surface tension and the adhesion to the SWCNT thin film substrate. Therefore, viscosity properties of dispersions were taken into account in determining the volumetric ratio of the given dispersions to prepare SWCNT/PEDOT:PSS thin films.

Table 5.3 : Properties of PEDOT:PSS Dispersions in Water

Trade name	Solids Content in Water (wt %)	PEDOT:PSS Ratio (wt %)	Viscosity (mPa.s, 20 °C)	Electrical Conductivity (S/cm)
Clevios PH 1000	1-1.3	1:2.5	15-60	850*
Clevios PH 500	1-1.3	1:2.5	8-25	300*
Clevios FET	3-4	N/A	20-80	200

* Conductivities for Clevios PH1000 and PH500 are measured for dispersions that contain of 5% DMSO.

Moreover, in Heraeous PEDOT:PSS data sheets, conductivity values for PH 1000 and 500 dispersions were measured as 850 and 300 S/cm respectively, which also contained DMSO in their dispersions. Thus, the effect of DMSO was also studied for both dispersions.

The surface tension and adhesion of a substrate are two key factors to fabricate uniform thin films with the spin coating method. Particularly, the viscosity of the fluid and the hydrophilic or hydrophobic tendency of the substrate heavily influence the film quality. In order to address and tackle these problems, each PEDOT:PSS dispersion was first coated onto SWCNT thin film without diluting with DI water. Table 5.4 compares the optoelectronic properties of SWCNT/PEDOT:PSS thin films with different volumetric ratios. The experimental procedure of SWCNT films were kept the same. For each type of dispersion SWCNT thin films with similar optoelectronic properties were selected for comparison.

The spin coating procedure was done by depositing two layers using 500 μL each and the spin coating sequence was kept the same for each film. The first attempt was done by using PH 1000 on Sample 1. The first 500 μL layer resulted a decrease of approximately 30% in sheet resistance, while the second layer resulted in another 20% decrease within the thin film. Interestingly, the sheet resistance measurements were taken again 1 week later which resulted in additional decrease of approximately 20%. The optical transparency of the thin film showed change from 82.2 % to 74%, which had the obvious hints PEDOT:PSS distinctive blue color.

Table 5.4 : Evaluation of SWCNT/PEDOT:PSS thin films with different PEDOT:PSS/DI Water ratios.

#	Trade name of PEDOT:PSS	PEDOT:PSS /DI Water ratio	$R_{s\ before}$ (Ω/sq)	$R_{s\ after}$ (Ω/sq)	T_{before} (%)	T_{after} (%)
1	PH 1000	1:0	1000	350	82.2	74
2	PH 1000	1:1	1000	400	77.1	72
3	PH 500	1:0	550	340	82	79
4	FET	1:0	517	100	78	43
5	FET	1:1	580	142	81.3	55

Despite the electronic properties of sample 1 turned out to be extremely well with 350 Ω/sq in sheet resistance, the film quality after the 2nd deposition of PEDOT:PSS deteriorated the SWCNT thin film structure almost instantly. As mentioned above, the purpose of this study was to avoid issues regarding film quality. Thus, a second approach was conducted with PH 1000 by diluting the dispersion with DI water (1:1). The diluted PH 1000 solution was spin coated with the same experimental procedure as Sample 1 and the sheet resistance decreased from 1 k Ω/sq to 400 Ω/sq. Due to dilution with water, the transparency value of the film showed slight decrease than Sample 1. However, this approach did not prevent the film from being damaged. Moreover, both films showed very similar effects of surface damages that occurred in HNO_3 treatments on SWCNT thin films. This similarity could be attributed to the acidity of PEDOT:PSS. The commercial Clevios PH 1000 has a strong acidic nature with a pH level between 1.5-2.5, which can be explained by the presence of sodium polysterene sulfonate (PSS). The PSS chains of the PEDOT:PSS polymer contains SO_3H groups that releases H^+ ions into the dispersions of water, which evidently gives its acidic property and leads to poor stability in composite thin films [120].

For sample 3, Clevios PH 500 was used to fabricate SWCNT/PEDOT:PSS thin films. In comparison to films sample 1-2 which were fabricated with PH 1000, the damages of the SWNCT film caused by the acid corrosion was much less. The sheet resistance was measured as 340 Ω/sq after the addition of PH 500, showing a 38% decrease in total. However, since dilution with DI water would have reduced the effect on the sheet resistance, this step was not conducted on PH 500.

On the other hand, Clevios FET showed a better performance in wettability and overall film quality compared to PH 1000. As seen in Table 5.3 , the high viscosity of Clevios FET dispersion made it possible to spread easily across the SWCNT film. During and

after fabrication, there were no visible distruptions on the surface. While the fabricated Sample 3 showed a sheet resistance decrease from 517 Ω/sq to 110 Ω/sq.

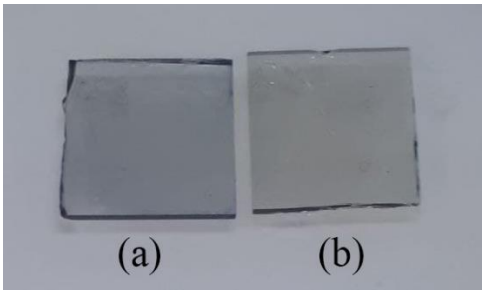

Figure 5.11 : Optical transparency comparison of (a) SWCNT/PEDOT:PSS and (b) SWCNT thin films.

There was a drastic change in optical transparency from 78% to 43% as seen in Figure 5.11. Thus, the Clevios FET concentration was diluted to 1:1 using DI water. While the sheet resistance did not change significantly after dilution with DI water, the optical transparency was somewhat more improved than sample 3. Despite this improvement, undoubtedly the optical transparency is nowhere near to the ITO's transparency results.

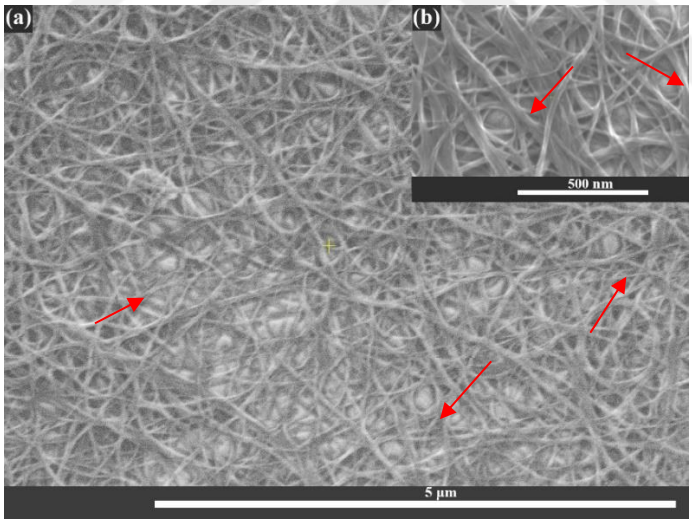

Figure 5.12 : SEM images of SWCNT/PEDOT:PSS nanocomposites at (a) 5 µm and (b) 500 nm.

SEM images of SWCNT/PEDOT:PSS using Clevios FET are illustrated in Figure 5.12. Dense network of SWCNTs are visible over the whole surface of the film. In contrast to the SEM images of the SWCNT films, Figure 5.12 reveals that the vacancies between nanotubes are almost entirely filled with spherical particles of PEDOT: PSS, which are pointed out with arrows. This could indicate that the surface roughness might have been reduced.

According to Crispin et al., the grains of PEDOT:PSS have the typical grain size of 20-25 nm, with shapes that resemble flattened balls or pancakes [121]. The morphology is most likely the outcome of the spin coating technique, during which thickness of the film diminishes as the water evaporates from the surface while the film remains intact in the lateral direction.

5.2.1.2 Effect of DMSO in SWCNT/PEDOT:PSS nanocomposites

Research on PEDOT:PSS have shown that the addition of high boiling solvents such as EG [122], [123], sorbitol [124], [125] and DMSO [126] improve the electronic properties of PEDOT:PSS to the formulation. These solvents prove to decrease the optical transparency by eliminating PSS out of PEDOT:PSS, since PSS possesses insulating properties in PEDOT:PSS [127]–[131].

Many efforts have been made to increase the electrical conductivity treating especially with DMSO [127], [128], [131]. Thus, in this study, the effects of DMSO improvements on the electrical conductivity of films with PH 500 and FET were studied.

Table 5.5 : Optoelectronic properties of SWCNT/PEDOT:PSS with/without DMSO treatment.

#	Trade name of PEDOT:PSS	DMSO volume (μL)	$R_{s\ before}$ (Ω/sq)	$R_{s\ after}$ (Ω/sq)	T_{before} (%)	T_{after} (%)
1	PH500	0	550	340	82	79
2	PH500	50	550	168	84	78.4
3	FET	0	580	142	81.3	55
4	FET	50	580	430	80.2	63.2

Table 5.5 shows the optoelectronic properties of SWCNT/PEDOT:PSS films. Sample 2 shows after the DMSO post treatment, the PH 500 films are drastically improved in sheet resistance. Without this treatment, the PH 500 films were only decreased to a sheet resistance of 340 Ω/sq whereas after treatment the film resistance showed 168 Ω/sq. DMSO improvement also had a small effect on transparency with a decrease of approximately 6%, in comparison to sample 1. Regardless of these results, the wettability of the PH 500 solution was still challenging and the overall film quality was not as high as expected.

In the meantime, sample 4 showed an opposite effect with DMSO treatment, where the resistance reduced less than that of the untreated films of FET. These results were found to be consistent with other studies done in literature that used DMSO treatment [132]–[134]. The change in conductivity is elaborated by the partial phase separation of the insulating PSS chains from the PEDOT:PSS domains. More specifically, the oxygen in ambient air plays an important role with DMSO, which allows it to incorporate into the grain boundaries of the PEDOT:PSS as defects and forms pathways for charge transport [120], [121], [128], [132], [134], [135]. The opposite effect of DMSO in PH 500 and FET can be explained by their average grain size which is 110 and 40 nm, respectively [136]. According to Cruz-Cruz et al. AFM and impedance spectroscopy of the treated and untreated PEDOT:PSS results, as DMSO concentration increases, not only the conducting PEDOT boundaries increase, but also the insulating barriers change in thickness. In our case, the addition of DMSO in FET samples increased the PEDOT polymer grain size while the PSS insulating chains also increased in thickness.

5.2.2 Evaluation of SWCNT/AgNW TCFs

To synthesize high performance AgNW films, the nanowire length, diameter and aspect ratio plays an important role in the AgNW network. While the long NWs exhibit good electrical conductivity, the diameter is particularly cruical in determining the optical transparency, haze factor and flexibility for the nanowires. Therefore, the synthesis for an optimum AgNW process should yield ultra-long and ultra-thin nanowires with a large aspect ratio.

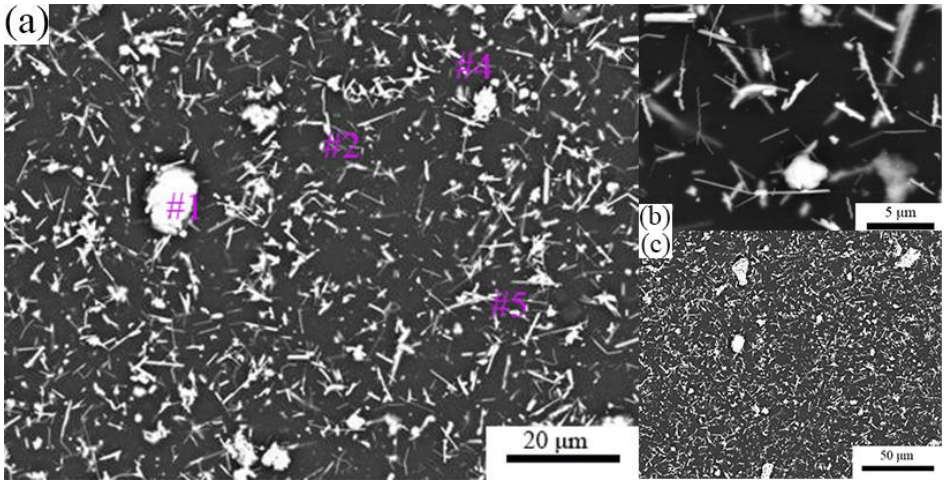

Figure 5.13 : EDX and SEM results of AgNW in (a) EDX and (b),(c) SEM respectively.

AgNWs with lengths up to 20 μm and an average diameter of 20 nm can be obtained by polyol synthesis [137], [138]. However up until now, only commercial AgNWs have proven to exceed the optoelectronic properties of ITO [139].The characteristics of the provided AgNW powder are given in Figure 5.13, where (a) represents the EDX image with numbered placemarks. Each placemark's respective elemental analysis is given in Table 5.6. The visible large agglomerate numbered as #1 is seen in Figure 5.13 which contains 84.3 % of Ag element according to Table 5.6. This means that the concentration of $AgNO_3$, which is the precursor of AgNWs, could have been excess in comparison to the reduction agents concentration.

Table 5.6 : EDX analysis results of AgNW powder.

Placemark	ELEMENTS								
	Ag	C	O	Si	Al	S	Ca	Na	Cl
#1	84.3	2	3.9	-	3.8	1.6	-	-	8.2
#2	59.6	14.4	16.1	5.2	1.6	3.1	-	-	-
#3	49.8	7.1	15.2	11.8	2.8	4.8	2.6	0.7	5.2
#4	46.8	16.3	15.7	9.2	3.2	5.5	2.8	0.5	-

Since the amount of reduction agents were too low to produce individual AgNWs, bulk nanoparticles have emerged such as #1 in Figure 5.13 (a). Other bulk nanoparticles are also visible in Figure 5.13 (b) and (c). The average length of the AgNWs were measured between the range of 2-5 μm and it is important to mention, as the $AgNO_3$ precursor concentration increases, the average length and diameter of the nanowires become shorter and wider respectively, which is consistent with other reported works [138], [140]. As seen in Figure 5.13 (c), even at the lowest magnification, the synthesized AgNWs are too short in length to form a functional network.

As evident by the EDX and SEM data, the integration of AgNW into the SWCNT ink had no significant effect on the sheet resistance values when compared to SWCNT and SWCNT/PEDOT:PSS films. The lowest sheet resistance of SWCNT/AgNW TCF showed approximately 385 Ω/sq, while the highest was measured as 645 Ω/sq, with respective optical transparencies of approximately 81% at the visible range.

5.2.3 Evaluation of SWCNT-AgNW-PEDOT:PSS nanocomposite TCFs

As mentioned in the experimental procedure, 2 strategies were followed with the nanocomposite fabrication. The first strategy was conducted as follows, 0.05 mg of AgNW powder was added into the FET dispersion (1:1) followed by spin coating the solution (1 ml) on top of the SWCNT film. As a result SWCNT/FET-AgNWs were obtained from the procedure. Table 5.7 shows the optoelectronic properties of the nanocomposite films and the first 2 samples belong to the procedure mentioned above. The sheet resistances are measured to be 430 Ω/sq and 400 Ω/sq for sample 1 and 2 respectively.

Table 5.7 : Optoelectronic properties of the fabricated nanocomposite TCFs.

#	Configuration	AgNW incorporation	Method of AgNW deposition	R_s (Ω/sq)	T (%)
1	SWCNT/FET-AgNW	PEDOT:PSS/DI water	Spin coating	430	37
2	SWCNT/FET-AgNW	PEDOT:PSS/DI water	Spin coating	400	60
3	SWCNT-AgNW/FET	SWCNT/NMP	Spray coating	219.5	59
4	SWCNT-AgNW/FET	SWCNT/NMP	Spray coating	250	61.4

In comparison to SWCNT/PEDOT:PSS, electrical conductivities are somehow lower. The AgNWs does not seem to be in effect with the samples. The low sheet resistance could be a part of the nano-welding of AgNWs occured by PEDOT:PSS. It is also important to mention that the AgNWs should not be expected to show high conductivity since the EDX and SEM analyses results conclude that the synthesized nanowires have small nanowire lengths and little to no wire-wire network interaction.

The second strategy was carried out by adding the same amount of AgNWs to the centrifuged SWCNT/NMP ink. The ink was deposited onto clean substrates which formed SWCNT- AgNW films. The temperature of the hotplate, nozzle to substrate distance, spray coating pressure and volume were kept the same as the SWCNT films. Afterwards, the diluted FET solution was spin coated and the films were annealed by a heater that was fixed to 120 °C. There were uncertainties whether the HNO_3 treatment could potentially cause acid corrosion on AgNWs as it happened with PEDOT:PSS. To avoid this, the chemical post treatments were not conducted on any of the nanocomposite films. The sheet resistance of these films are better than the previous samples, however the values are still not as low as its expected with the

addition of AgNWs. The best performing nanocomposite film shows a resistance of 219.5 Ω/sq, which is still very high compared to other studies done in literature.

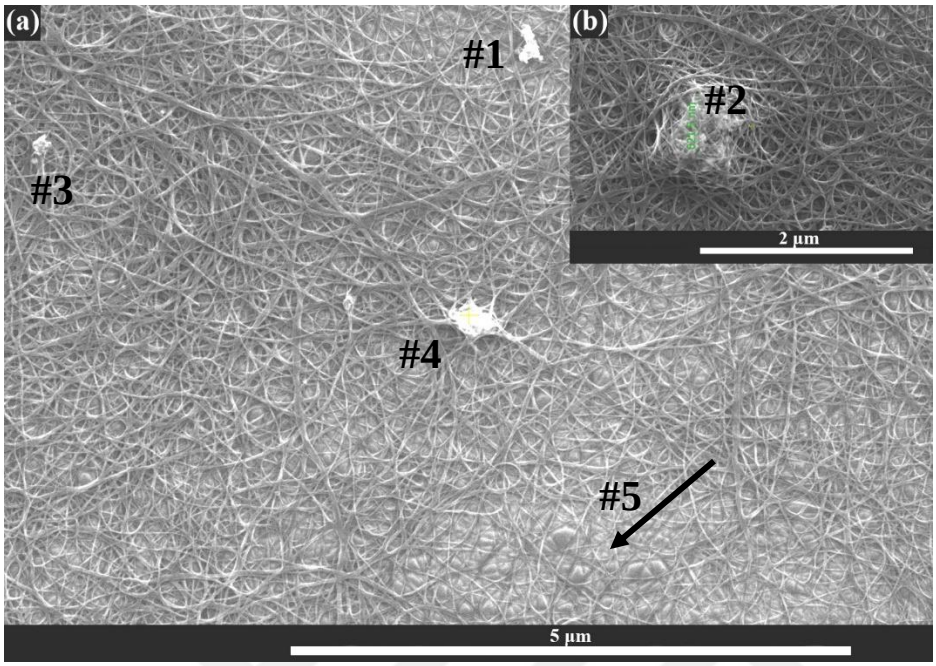

Figure 5.14 : SEM images of SWCNT-AgNW/FET nanocomposite (a) at 5 µm and (b) 2 µm.

The SEM images of SWCNT-AgNW/FET TCFs illustrated in Figure 5.14 show similar clusters of AgNW agglomerates that are shown in placemarks # 1,# 2,# 3 and # 4. These structures appear to be surrounded by nanotubes, as if they are embedded in the morphological structure. Nevertheless, the presence of nanowires are not visible which could be associated with the AgNW's short aspect ratios. The presence of PEDOT:PSS is also observed by their distinctive pancake-shaped grains, indicated at # 5.

6. CONCLUSIONS AND RECOMMENDATIONS

The final chapter of this thesis provides a summary of all results in the conclusions, and the recommendations section presents helpful insights for future studies of nanocomposites.

6.1 Conclusions

The aim of this thesis was to fabricate highly conductive and transparent nanocomposites using SWNCTs, AgNWs and PEDOT:PSS nanomaterials. In order to avoid the disadvantages that may occur between materials and to ensure compatibility the nanomaterials were optimized.

Each materials had its own set of chemical/physical problems in the film formation process.

- Commercial Tuball SWCNTs were were treated with HNO_3 solution with the concentration of 3M for 3h in order to improve the purity and remove metal catalysts. The purified SWCNT powder resulted in 12% decrease of metal impurities after treatment.
- Due to SWCNTs hydrophobicity, the glass substrates were treated with piranha solution. The effect of concentration, spray volume and spray pressure was particularly important to obtain highly uniform and conductive SWCNT thin films. The parameters were extensively studied and repeated over and over again to achieve repeatable results of SWCNT thin films.
- Spray coating technique parameters were optimized by comparing the optoelectronic properties of SWCNT films. SWCNT/NMP solutions at different concentrations (0.1, 0.2, 0.3 mg/ml) were prepared for the spray process at different carrier gas pressures (2, 3 and 4 bar) and volumes (1, 1.5 and 2 ml) to investigate the effects on the transparent thin films. The films fabricated with 0.1 mg/ml SWCNT/NMP solution under 2 bar carrier gas pressure using 1.5 ml spray volume showed the best performance.

- Post treatment methods of SWCNT films were also studied in this thesis, however it was not executed in nanocomposite film formation due to the surface damages caused by HNO_3. There were no definitive results that show whether $SOCl_2$ has inferior/superior qualities to improve the SWCNT thin films in comparison to HNO_3. Therefore, in light of FOM calculations both of the chemicals were considered to be effective in the post treatment methods. Far too little attention has been paid to the effect of $SOCl_2$ on electrical conductivity in SWCNT in literature [115], [117] to describe the mechanisms involving the SWCNT electronic structure.
- Due to PEDOT:PSS's acidity, the SWCNT film formation was abruptly affected by the acid corrosion of the conductive polymer. In particular, PH 1000 corrupted the surface almost immediately after the solution was spread onto the SWCNT film surface. PH 500 had a similar albeit lesser effect of acid corrosion to the surface, however, the initial coating of PEDOT: PSS did not show a drastic change in sheet resistance. FET showed better wettebility and film formation on the SWCNT surface in comparison to other dispersions of PEDOT:PSS, however, in this case due to FETs high viscosity, the optical transparency was excessively decreased. The sharp decrease in optical transparency is most likely due to the amount of solid PEDOT in the FET dispersion, which explains its high viscosity [120]. This assumption can be easily made because PSS polymer is mainly colorless and the distinctive blue tint of PEDOT:PSS comes from the PEDOT back bone.
- In light of these results explained for PEDOT:PSS dispersions, the PH 1000 was eliminated and the effect of DMSO was studied for both PH 500 and FET samples to improve their electronic properties. For the PH 500 samples, the DMSO treatment was effective in increasing the overall conductivity while FET showed an opposite behavior in electrical conduction to this post-treatment. This behavior was found to be consistent with other previous works done in PEDOT:PSS post-treatments, and is explained by the partial phase separation of the insulating PSS chains from the PEDOT:PSS domains.
- To put it bluntly, the AgNWs were planned to be purchased commercially in order to fabricate nanocomposites with superior performance. However, due to the corona virus pandemic the first restrictions began between March 16 and

June 1, 2020 and during this period, work permits in laboratories were revoked. After the initial restrictions of the pandemic virus were lifted, it could not be purchased due to the rising exchange rate and the expense of the AgNW nanomaterial. Therefore, synthesized AgNWs were provided from another research group. Unfortunately, no information could be obtained on how AgNW structures were synthesized. However, the EDX and SEM analyses of the powder gave important insights to this work. The length of the nanowires were measured to be approximately around 2-5 μm which was extremely small according to other works that were published. Moreover, the nanowire lengths were not long enough to form a conductive pathway within the nanowire mesh. In this regard it can be said that the provided AgNWs show very low conductivity.

- As a side note, to finish this thesis study, the PEDOT:PSS dispersions were provided from another researcher which I am thankful for. Nonetheless, our resources to PEDOT:PSS dispersions were very limited so we could not waste a single sample of PEDOT:PSS for an analysis.

6.2 Recommendations

- In light of the results that were obtained from this thesis, it can be determined that SWCNT thin films are only physically deposited onto the glass surface, which means there was no force or bond to attach the nanotube bundles onto the substrate. For this reason, SWCNT thin films were particularly very hard to work with. This may be among one of the causes of the reoccuring defects in chemical treatments, although not entirely due to SWCNT's adhesion to the surface. For future studies, the SWCNTs can be embedded into a polymer matrix as a solution to this problem.
- The spray coating technique was utilized to fabricate SWCNT thin films due to its simplicity. However, spray coating was done by the help of an airbrush, which was extremely time consuming to fabricate repeatable results and optimize the process for uniform thin films due to its manual use. Each film needed to be spray coated one at a time and nozzle to substrate distance was maintained by a lab stand. Nevertheless, the spray coating process is still a

great method to obtain highly conductive and transparent SWCNT thin films as shown in this thesis. However, the process could be simplified for researchers and the results can be improved with the help of an an automatic spray coating system .

- According to several studies, HNO_3 treatment can also be effective in reducing sheet resistance of PEDOT:PSS films as well as SWCNT thin films. Since HNO_3 treatment can remove PSS chains from PEDOT:PSS, the combined improvements from both materials could be obtained by a simple HNO_3 post treatment step [141][142]. This can also eliminate problems with SWCNT deterioration, since HNO_3 treatment can be used on top of PEDOT:PSS instead of directly treating SWCNT thin films.
- A safer way to improve the overall electrical conductivity is to treat PEDOT:PSS films with sorbitol or glycerol, instead of using highly toxic chemicals such as DMSO or EG. Sorbitol and glycerol has proven to be great post treatment chemicals to decrease the sheet resistance according to many studies done in the literature [128] [143][144][145].
- High surface roughness is another important problem for applications. To smoothen PEDOT:PSS films, methanol can also be used by spin coating onto fabricated the PEDOT:PSS films.
- Long term stabilites of PEDOT:PSS still remain as a big drawback in studies particularly where the films are fabricated as transparent conductive electrodes or hole transport layers in photovoltaic technologies. Since PEDOT:PSS is hygroscopic, it draws moisture from ambient air and this phenomena causes significant loss in electrical conductivity of the electrode. The increase of resistivity can be slowed down significantly using two strategies. The first step is to use protective layer on top of the PEDOT:PSS electrode to prevent the contact with ambient air using glass plates polymer coatings such as Clevios Al 4038 [13]. Encapsulating the PEDOT:PSS electrodes properly will delay the degradation of the film. In addition, stabilizing agents can be used to remove residual water in the PEDOT:PSS electrode by drying in a chamber under high vacuum [120].

- AgNWs are affected by the acid corrosion of PEDOT:PSS, therefore conductivity deterioration of AgNWs needs to be improved. There are other creative strategies for fabricating nanocomposites to resolve the damages in nanowires such as protecting the nanowire mesh with polyvinyl alcohol or burying into the PEDOT:PSS complex to form a hybrid nanomaterial [146]–[148].

REFERENCES

[1] **D. Levy and E.** (2018). Castellón, *Transparent Conductive Materials*. Wiley-VCH Verlag.

[2] **Y. Zhou and R. Azumi,** (2016). "Carbon nanotube based transparent conductive films: progress, challenges, and perspectives," *Sci. Technol. Adv. Mater.*, vol. 17, no. 1, pp. 493–516.

[3] **H. Liu, V. Avrutin, N. Izyumskaya, Ü. Özgür, and H. Morkoç,** (2010). "Transparent conducting oxides for electrode applications in light emitting and absorbing devices," *Superlattices Microstruct.*, vol. 48, no. 5, pp. 458–484, Nov.

[4] **C. Viespe, I. Nicolae, C. Sima, C. Grigoriu, and R. Medianu,** (Oct. 2007). "ITO thin films deposited by advanced pulsed laser deposition," *Thin Solid Films*, vol. 515, no. 24, pp. 8771–8775,

[5] **M. Layani, A. Kamyshny, and S. Magdassi,** (2014) "Transparent conductors composed of nanomaterials," *Nanoscale*, vol. 6, no. 11, pp. 5581–5591,.

[6] **S. Park, M. Vosguerichian, and Z. Bao,** (2013). "A review of fabrication and applications of carbon nanotube film-based flexible electronics," *Nanoscale*, vol. 5, no. 5, pp. 1727–1752,

[7] **F. Soltani-kordshuli, F. Zabihi, and M. Eslamian,** (2016). "Graphene-doped PEDOT:PSS nanocomposite thin films fabricated by conventional and substrate vibration-assisted spray coating (SVASC)," *Eng. Sci. Technol. an Int. J.*, vol. 19, no. 3, pp. 1216–1223,

[8] **D. Liu *et al.*,** (2017). "Improved performance of inverted planar perovskite solar cells with F4-TCNQ doped PEDOT:PSS hole transport layers," *J. Mater. Chem. A*, vol. 5, no. 12, pp. 5701–5708,

[9] **M. Yi, W. Jang, and D. H. Wang,** (2019). "Controlled pH of PEDOT:PSS for Reproducible Efficiency in Inverted Perovskite Solar Cells: Independent of Active Area and Humidity," *ACS Sustain. Chem. Eng.*, vol. 7, no. 9, pp. 8245–8254, May

[10] **S. Razza *et al.*,** (2015). "Perovskite solar cells and large area modules (100 cm 2) based on an air flow-assisted PbI 2 blade coating deposition process," *J. Power Sources*,.

[11] **R. Treharne, L. Phillips, J. Major, S. V. Farahani, T. Veal, and K. Durose,** "Transparent conducting oxides for thin film PV TCOs in solar cells."

[12] **A. Stadler,** (2012). "Transparent Conducting Oxides—An Up-To-Date Overview," *Materials (Basel).*, vol. 5, no. 12, pp. 661–683,

[13] **A. Elschner, S. Kirschmeyer, W. Lövenich, U. Merker, and K. Reuter,** (2013). *PEDOT: Principles and Applications of an Intrinsically Conductive Polymer*, vol. 53, no. 9.

[14] **J. T. Littleton,** (1931). "US Patent 2118795,"

[15] **D. S. Hecht, L. Hu, and G. Irvin,** (2011). "Emerging Transparent Electrodes Based on Thin Films of Carbon Nanotubes , Graphene , and Metallic Nanostructures," *Adv. Mater.*, vol. 23, no. 13, pp. 1482–1513, Apr.

[16] **Q. Bu, Y. Zhan, F. He, M. Lavorgna, and H. Xia,** (2016). "Stretchable conductive films based on carbon nanomaterials prepared by spray coating," *J. Appl. Polym. Sci.*, vol. 133, no. 15, pp. 1–8,

[17] **R. Gupta, K. D. M. Rao, S. Kiruthika, and G. U. Kulkarni,** (2016). "Visibly Transparent Heaters," *ACS Appl. Mater. Interfaces*, vol. 8, no. 20, pp. 12559–12575,

[18] **A. Kaskela *et al.*,** (2016). "Highly individual SWCNTs for high performance thin film electronics," *Carbon N. Y.*, vol. 103, pp. 228–234,

[19] **H. W. C. Postma, T. Teepen, Z. Yao, M. Grifoni, and C. Dekker,** (2001). "Carbon nanotube single-electron transistors at room temperature," *Science (80-.).*, vol. 293, no. 5527, pp. 76–79,

[20] **R. H. Baughman *et al.*,** (1999). "Carbon nanotube actuators," *Science (80-.).*, vol. 284, no. 5418, pp. 1340–1344,

[21] **Q. H. Wang, A. A. Setlur, J. M. Lauerhaas, J. Y. Dai, E. W. Seelig, and R. P. H. Chang,** (1998). "A nanotube-based field-emission flat panel display," *Appl. Phys. Lett.*, vol. 72, no. 22, pp. 2912–2913,

[22] **K. A. Dean and B. R. Chalamala,** (1999). "Field emission microscopy of carbon nanotube caps," *J. Appl. Phys.*, vol. 85, no. 7, pp. 3832–3836,

[23] **P. G. Collins and A. Zettl,** (1996). "A simple and robust electron beam source from carbon nanotubes," *Appl. Phys. Lett.*, vol. 69, no. 13, pp. 1969–1971,

[24] **B. J. Yoon, S. H. Jeong, K. H. Lee, H. Seok Kim, C. Gyung Park, and J. Hun Han,** (2004). "Electrical properties of electrical double layer capacitors with integrated carbon nanotube electrodes," *Chem. Phys. Lett.*, vol. 388, no. 1–3, pp. 170–174,

[25] **J. Lee *et al.*,** (2017). "Transparent, Flexible Strain Sensor Based on a Solution-Processed Carbon Nanotube Network," *ACS Appl. Mater. Interfaces*, vol. 9, no. 31, pp. 26279–26285,

[26] **A. Albrecht *et al.*,** (2017). "Transparent Thermocouples based on Spray-coated Nanocomposites," pp. 7–9,

[27] **M. Ding, Y. Tang, P. Gou, M. J. Reber, and A. Star,** (2011). "Chemical sensing with polyaniline coated single-walled carbon nanotubes," *Adv. Mater.*, vol. 23, no. 4, pp. 536–540, Jan.

[28] **L. He and S. C. Tjong,** (2016). "Nanostructured transparent conductive films: Fabrication, characterization and applications," *Mater. Sci. Eng. R Reports*, vol. 109, pp. 1–101, Nov.

[29] **D. Langley, G. Giusti, C. Mayousse, C. Celle, D. Bellet, and J.-P. Simonato,** (2013). "Flexible transparent conductive materials based on silver nanowire networks: a review," *Nanotechnology*, vol. 24, no. 45, p. 452001, Nov.

[30] **M. Azani, A. Hassanpour, and T. Torres,** (2020). "Benefits , Problems , and Solutions of Silver Nanowire Transparent Conductive Electrodes in Indium Tin Oxide (ITO) -Free Flexible Solar Cells," vol. 2002536, pp. 1–32,

[31] **X. Huang, Z. Zeng, Z. Fan, J. Liu, and H. Zhang,** (2012). "Graphene-based electrodes," *Adv. Mater.*, vol. 24, no. 45, pp. 5979–6004,

[32] **K. Ellmer,** (2012). "development of optically transparent electrodes," *Nat. Photonics*, vol. 6, no. November,

[33] **D. B. Fraser and H. D. Cook,** (1972). "Highly Conductive, Transparent Films of Sputtered In[sub 2−x]Sn[sub x]O[sub 3−y]," *J. Electrochem. Soc.*, vol. 119, no. 10, p. 1368,

[34] **G. Haacke,** (1976). "New figure of merit for transparent conductors," *J. Appl. Phys.*, vol. 47, no. 9, pp. 4086–4089,

[35] **J. Prasek *et al.*,** (2011). "Methods for carbon nanotubes synthesis - Review," *J. Mater. Chem.*, vol. 21, no. 40, pp. 15872–15884,

[36] **S. A. Hodge, M. K. Bayazit, K. S. Coleman, and M. S. P. Shaffer,** (2012). "Unweaving the rainbow: A review of the relationship between single-walled carbon nanotube molecular structures and their chemical reactivity," *Chem. Soc. Rev.*, vol. 41, no. 12, pp. 4409–4429,

[37] **L. Yu, C. Shearer, and J. Shapter,** (2016). "Recent Development of Carbon Nanotube Transparent Conductive Films," *Chem. Rev.*, vol. 116, no. 22, pp. 13413–13453,

[38] **K. K. Kim, S. M. Kim, and Y. H. Lee,** (2016). "Chemically Conjugated Carbon Nanotubes and Graphene for Carrier Modulation," *Acc. Chem. Res.*, vol. 49, no. 3, pp. 390–399,

[39] **P. Kim, T. W. Odom, J. L. Huang, and C. M. Lieber,** (1999). "Electronic density of states of atomically resolved single-walled carbon nanotubes: Van hove singularities and end states," *Phys. Rev. Lett.*, vol. 82, no. 6, pp. 1225–1228,

[40] **X. Liu *et al.*,** (2002). "Detailed analysis of the mean diameter and diameter distribution of single-wall carbon nanotubes from their optical response," *Phys. Rev. B - Condens. Matter Mater. Phys.*, vol. 66, no. 4, pp. 454111–454118,

[41] **W. Ma, L. Song, R. Yang, T. Zhang, and Y. Zhao,** (2007). "Directly Synthesized Strong, Highly Conducting, Transparent Single-Walled Carbon Nanotube Films," *Nano Lett.*,

[42] **F. Bonaccorso, Z. Sun, T. Hasan, and A. C. Ferrari,** (2010). "Graphene photonics and optoelectronics," *Nat. Photonics*, vol. 4, no. 9, pp. 611–622,

[43] **L. Hu, D. S. Hecht, and G. Grüner,** (2010). "Carbon nanotube thin films: Fabrication, properties, and applications," *Chem. Rev.*, vol. 110, no. 10, pp. 5790–5844,

[44] **H. Wang,** (2009). "Dispersing carbon nanotubes using surfactants," *Curr. Opin. Colloid Interface Sci.*, vol. 14, no. 5, pp. 364–371,

[45] **A. Bstract,** "A Study of the Dispersion and Debundling of Single Walled Carbon Nanotubes."

[46] **Y. Kuwahara, T. Hirai, and T. Saito,** (2018). "Effects of tube diameter and length on transparent conductivity of single-walled carbon nanotube network films," *J. Nanomater.*, vol. 2018,

[47] **J. Gao, W. Y. Wang, L. T. Chen, L. J. Cui, X. Y. Hu, and H. Z. Geng,** (2013). "Optimizing processes of dispersant concentration and post-treatments for fabricating single-walled carbon nanotube transparent conducting film," *Appl. Surf. Sci.*, vol. 277, pp. 128–133,

[48] **M. S. Strano *et al.*,** (2003). "The Role of Surfactant Adsorption during Ultrasonication in the Dispersion of Single-Walled Carbon Nanotubes," *J. Nanosci. Nanotechnol.*, vol. 3, no. 1, pp. 81–86,

[49] **Y. Wang and B. Fugetsu,** (2015). "Mono-dispersed ultra-long single-walled carbon nanotubes as enabling components in transparent and electrically conductive thin films," *Carbon N. Y.*, vol. 82, no. C, pp. 152–160,

[50] **K. Lee, H. J. Lim, S. J. Yang, Y. S. Kim, and C. R. Park,** (2013). "Determination of solubility parameters of single-walled and double-walled carbon nanotubes using a finite-length model," *RSC Adv.*, vol. 3, no. 14, pp. 4814–4820,

[51] **K. K. Kim *et al.*,** (2007). "Design of dispersants for the dispersion of carbon nanotubes in an organic solvent," *Adv. Funct. Mater.*, vol. 17, no. 11, pp. 1775–1783, Jul.

[52] **S. Giordani *et al.*,** (2006). "Debundling of single-walled nanotubes by dilution: Observation of large populations of individual nanotubes in amide solvent dispersions," *J. Phys. Chem. B*, vol. 110, no. 32, pp. 15708–15718,

[53] **H. C. Yau, M. K. Bayazit, J. H. G. Steinke, and M. S. P. Shaffer,** (2015). "Sonochemical degradation of N-methylpyrrolidone and its influence on single walled carbon nanotube dispersion," *Chem. Commun.*, vol. 51, no. 93, pp. 16621–16624,

[54] **J. L. Bahr, E. T. Mickelson, M. J. Bronikowski, R. E. Smalley, and J. M. Tour,** (2001). "Dissolution of small diameter single-wall carbon nanotubes in organic solvents?," *Chem. Commun.*, no. 2, pp. 193–194,

[55] **A. Hirano, Y. Maeda, T. Akasaka, and K. Shiraki,** (2009). "Synergistically enhanced dispersion of native protein-carbon nanotube conjugates by fluoroalcohols in aqueous solution," *Chem. - A Eur. J.*, vol. 15, no. 38, pp. 9905–9910,

[56] **O. Matarredona, H. Rhoads, Z. Li, J. H. Harwell, L. Balzano, and D. E. Resasco,** (2003). "Dispersion of Single-Walled Carbon Nanotubes in Aqueous Solutions of the Anionic Surfactant NaDDBS," *J. Phys. Chem. B*, vol. 107, no. 48, pp. 13357–13367,

[57] **B. Sohrabi, N. Poorgholami-Bejarpasi, and N. Nayeri,** (2014). "Dispersion of carbon nanotubes using mixed surfactants: Experimental and molecular dynamics simulation studies," *J. Phys. Chem. B*, vol. 118, no. 11, pp. 3094–3103,

[58] **W. H. Duan, Q. Wang, and F. Collins,** (2011). "Dispersion of carbon nanotubes with SDS surfactants: A study from a binding energy perspective," *Chem. Sci.*, vol. 2, no. 7, pp. 1407–1413,

[59] **S. Azoz *et al.*,** (2015). "Enhanced dispersion and electronic performance of single-walled carbon nanotube thin films without surfactant: A comprehensive study of various treatment processes," *Carbon N. Y.*, vol. 93, pp. 1008–1020,

[60] **C. Preston *et al.*,** (2015). "Scalable nanomanufacturing of surfactant-free carbon nanotube inks for spray coatings with high conductivity," *Nano Res.*, vol. 8, no. 7, pp. 2242–2250,

[61] **S. D. Bergin *et al.*,** (2008). "Large populations of individual nanotubes in surfactant-based dispersions without the need for ultracentrifugation," *J. Phys. Chem. C*, vol. 112, no. 4, pp. 972–977,

[62] **M. F. Islam, E. Rojas, D. M. Bergey, A. T. Johnson, and A. G. Yodh,** (2003). "Solubilization of Single-Wall Carbon Nanotubes in Water," *Nano Lett.*, vol. 3, no. 2, pp. 269–273,

[63] **A. Martinez-Hernandez, C. Velasco-Santos, and V. Castano,** (2010). "Carbon Nanotubes Composites: Processing, Grafting and Mechanical and Thermal Properties," *Curr. Nanosci.*, vol. 6, no. 1, pp. 12–39,

[64] **B. M. A. Hamon, J. Chen, H. Hu, and Y. Chen,** (1999). "Dissolution of Single-Walled Carbon.pdf," vol. 0055, no. 10, pp. 834–840,

[65] **F. Liang *et al.*,** (2006). "Highly exfoliated water-soluble single-walled carbon nanotubes," *Chem. Mater.*, vol. 18, no. 6, pp. 1520–1524,

[66] **C. S. Woo *et al.*,** (2007). "Fabrication of flexible and transparent single-wall carbon nanotube gas sensors by vacuum filtration and poly(dimethyl siloxane) mold transfer," *Microelectron. Eng.*, vol. 84, no. 5–8, pp. 1610–1613,

[67] **B. King and B. Panchapakesan,** (2014). "Vacuum filtration based formation of liquid crystal films of semiconducting carbon nanotubes and high performance transistor devices," *Nanotechnology*, vol. 25, no. 17,

[68] **J. Wang, M. Liang, Y. Fang, T. Qiu, J. Zhang, and L. Zhi,** (2012). "Rod-coating: Towards large-area fabrication of uniform reduced graphene oxide films for flexible touch screens," *Adv. Mater.*, vol. 24, no. 21, pp. 2874–2878,

[69] **B. Dan, G. C. Irvin, and M. Pasquali,** (2009). "Continuous and Scalable Fabrication of Nanotube Films," *ACS Nano*, vol. 3, no. 4, pp. 835–843,

[70] **S. Azoz *et al.*,** (2015). "Highly conductive single-walled carbon nanotube thin film preparation by direct alignment on substrates from water dispersions," *Langmuir*, vol. 31, no. 3, pp. 1155–1163,

[71] **D. Y. Cho, K. Eun, S. H. Choa, and H. K. Kim,** (2014). "Highly flexible and stretchable carbon nanotube network electrodes prepared by simple brush painting for cost-effective flexible organic solar cells," *Carbon N. Y.*, vol. 66, pp. 530–538,

[72] **A. Abrishamchian, T. Hooshmand, M. Mohammadi, and F. Najafi,** (2013). "Preparation and characterization of multi-walled carbon nanotube/hydroxyapatite nanocomposite film dip coated on Ti-6Al-4V by sol-gel method for biomedical applications: An in vitro study," *Mater. Sci. Eng. C*, vol. 33, no. 4, pp. 2002–2010,

[73] **B. Dastorian Jamnani, S. Hosseini, S. Rahmanian, S. Abdul Rashid, S. B. Mustapha, and S. Keshan Balavandy,** (2015). "Grafting Carbon Nanotubes on Glass Fiber by Dip Coating Technique to Enhance Tensile and Interfacial Shear Strength," *J. Nanomater.*, vol. 2015,

[74] **X. Li, Q. Li, and G. X. Chen,** (2014). "Alkali metal surfactant-facilitated formation of thick boron nitride layers on carbon nanotubes by dip-coating," *Mater. Lett.*, vol. 134, pp. 38–41,

[75] **J. W. Jo, J. W. Jung, J. U. Lee, and W. H. Jo,** (2010). "Fabrication of highly conductive and transparent thin films from single-walled carbon nanotubes using a new non-ionic surfactant via spin coating," *ACS Nano*, vol. 4, no. 9, pp. 5382–5388, Sep.

[76] **E. Kymakis, M. M. Stylianakis, G. D. Spyropoulos, E. Stratakis, E. Koudoumas, and C. Fotakis,** (2012). "Spin coated carbon nanotubes as the hole transport layer in organic photovoltaics," *Sol. Energy Mater. Sol. Cells*, vol. 96, no. 1, pp. 298–301,

[77] **A. E. Ostfeld *et al.*,** (2014). "Single-walled carbon nanotube transparent conductive films fabricated by reductive dissolution and spray coating for organic photovoltaics," *Appl. Phys. Lett.*, vol. 105, no. 25, Dec.

[78] **R. C. Tenent *et al.*,** (2009). "UItrasmooth, large-area, high-uniformity, conductive transparent single-walled-carbon-nanotube films for photovoltaics produced by ultrasonic spraying," *Adv. Mater.*, vol. 21, no. 31, pp. 3210–3216,

[79] **S. Kim, J. Yim, X. Wang, D. D. C. Bradley, S. Lee, and J. C. DeMello,** (Jul. 2010). "Spin-and spray-deposited single-walled carbon-nanotube electrodes for organic solar cells," *Adv. Funct. Mater.*, vol. 20, no. 14, pp. 2310–2316,

[80] **S. Paul and D. W. Kim,** (2009). "Preparation and characterization of highly conductive transparent films with single-walled carbon nanotubes for flexible display applications," *Carbon N. Y.*, vol. 47, no. 10, pp. 2436–2441,

[81] **J. S. Woo, G. W. Lee, S. Y. Park, and J. T. Han,** (2017). "Realization of transparent conducting networks with high uniformity by spray deposition on flexible substrates," *Thin Solid Films*, vol. 638, pp. 367–374,

[82] **Z. Z. Gu, S. L. Jia, G. Li, C. Li, Y. Q. Wu, and H. Z. Geng,** (2019). "Mechanism of surface treatments on carbon nanotube transparent conductive films by three different reagents," *RSC Adv.*, vol. 9, no. 6, pp. 3162–3168,

[83] **Y. S. L. and C. O. Y. Y.W. Park, C. Park,** (1988). "ELECTRICAL CONDUCTIVITY OF HIGHLY-ORIENTED-POLYACETYLENE," *Solid State Commun.*, vol. 65, no. 2, pp. 147–150,

[84] **Y. W. Park, A. J. Heeger, M. A. Druy, and A. G. MacDiarmid,** (1980). "Electrical transport in doped polyacetylene," *J. Chem. Phys.*, vol. 73, no. 2, pp. 946–957,

[85] **G. J. Adekoya, O. C. Adekoya, R. E. Sadiku, and S. S. Ray,** (2021). "Structure-property relationship and nascent applications of thermoelectric PEDOT:PSS/carbon composites: A review," *Compos. Commun.*, vol. 27, no. August, p. 100890,

[86] **G. Greczynski, T. Kugler, and W. R. Salaneck,** (1999). "Characterization of the PEDOT-PSS system by means of X-ray and ultraviolet photoelectron spectroscopy," *Thin Solid Films*, vol. 354, no. 1, pp. 129–135,

[87] **H. Shi, C. Liu, Q. Jiang, and J. Xu,** (2015). "Effective Approaches to Improve the Electrical Conductivity of PEDOT : PSS : A Review," pp. 1–16,

[88] **S. Chen, B. Lu, X. Duan, and J. Xu,** (2012). "Systematic study on chemical oxidative and solid-state polymerization of poly(3,4-ethylenedithiathiophene)," *J. Polym. Sci. Part A Polym. Chem.*, vol. 50, no. 10, pp. 1967–1978,

[89] **S. Kirchmeyer and K. Reuter,** (2005). "Scientific importance, properties and growing applications of poly(3,4-ethylenedioxythiophene)," *J. Mater. Chem.*, vol. 15, no. 21, pp. 2077–2088,

[90] **Z. Wang, Z. Wang, H. Zhang, X. Duan, J. Xu, and Y. Wen,** (2015). "Electrochemical sensing application of poly(acrylic acid modified EDOT-co-EDOT):PSS and its inorganic nanocomposite with high soaking stability, adhesion ability and flexibility," *RSC Adv.*, vol. 5, no. 16, pp. 12237–12247,

[91] **M. N. Gueye, A. Carella, J. Faure-Vincent, R. Demadrille, and J. P. Simonato,** (2020). "Progress in understanding structure and transport properties of PEDOT-based materials: A critical review," *Prog. Mater. Sci.*, vol. 108, p. 100616,

[92] **A. G. MacDiarmid and A. J. Epstein,** (1994). "The concept of secondary doping as applied to polyaniline," *Synth. Met.*, vol. 65, no. 2–3, pp. 103–116,

[93] **S. K. M. Jönsson *et al.*,** (2003). "The effects of solvents on the morphology and sheet resistance in poly(3,4-ethylenedioxythiophene)-polystyrenesulfonic acid (PEDOT-PSS) films," *Synth. Met.*, vol. 139, no. 1, pp. 1–10,

[94] **G. Greczynski, T. Kugler, M. Keil, W. Osikowicz, M. Fahlman, and W. R. Salaneck,** (2001). "Photoelectron spectroscopy of thin films of PEDOT–PSS.pdf," vol. 121, pp. 1–17,

[95] **N. Kim *et al.*,** (2014). "Highly conductive PEDOT:PSS nanofibrils induced by solution-processed crystallization," *Adv. Mater.*, vol. 26, no. 14, pp. 2268–2272,

[96] **W. He and C. Ye,** (2015). "Journal of Materials Science & Technology Flexible Transparent Conductive Films on the Basis of Ag Nanowires : Design and Applications : A Review," *J. Mater. Sci. Technol.*, vol. 31, no. 6, pp. 581–588,

[97] **S. Ji, W. He, K. Wang, Y. Ran, and C. Ye,** (2014). "Thermal response of transparent silver nanowire/PEDOT:PSS film heaters," *Small*, vol. 10, no. 23, pp. 4951–4960,

[98] **S. M. Bergin, Y. H. Chen, A. R. Rathmell, P. Charbonneau, Z. Y. Li, and B. J. Wiley,** (2012). "The effect of nanowire length and diameter on the properties of transparent, conducting nanowire films," *Nanoscale*, vol. 4, no. 6, pp. 1996–2004,

[99] **S. Sorel, P. E. Lyons, S. De, J. C. Dickerson, and J. N. Coleman,** (2012). "The dependence of the optoelectrical properties of silver nanowire networks on nanowire length and diameter," *Nanotechnology*, vol. 23, no. 18,

[100] **R. M. Mutiso and K. I. Winey,** (2013). "Electrical percolation in quasi-two-dimensional metal nanowire networks for transparent conductors," *Phys. Rev. E - Stat. Nonlinear, Soft Matter Phys.*, vol. 88, no. 3, pp. 1–8,

[101] **L. Hu, H. S. Kim, J. Y. Lee, P. Peumans, and Y. Cui,** (2010). "Scalable coating and properties of transparent, flexible, silver nanowire electrodes," *ACS Nano*, vol. 4, no. 5, pp. 2955–2963,

[102] **J. Lee *et al.*,** (2013). "Room-temperature nanosoldering of a very long metal nanowire network by conducting-polymer-assisted joining for a flexible touch-panel application," *Adv. Funct. Mater.*, vol. 23, no. 34, pp. 4171–4176,

[103] **J. Li, J. Liang, X. Jian, W. Hu, J. Li, and Q. Pei,** (2014). "A flexible and transparent thin film heater based on a silver nanowire/heat-resistant polymer composite," *Macromol. Mater. Eng.*, vol. 299, no. 11, pp. 1403–1409,

[104] **D. Y. Shin *et al.*,** (2013). "Rapid two-step metallization through physicochemical conversion of Ag 2O for printed 'black' transparent conductive films," *Nanoscale*, vol. 5, no. 11, pp. 5043–5052,

[105] **L. Yang, T. Zhang, H. Zhou, S. C. Price, B. J. Wiley, and W. You,** (2011). "Solution-processed flexible polymer solar cells with silver nanowire electrodes," *ACS Appl. Mater. Interfaces*, vol. 3, no. 10, pp. 4075–4084,

[106] **L. José Andrés *et al.,*** (2015). "Rapid synthesis of ultra-long silver nanowires for tailor-made transparent conductive electrodes: proof of concept in organic solar cells," *Nanotechnology*, vol. 26, no. 26, pp. 1–9,

[107] **D. Janas and G. Stando,** (2017). "Unexpectedly strong hydrophilic character of free-standing thin films from carbon nanotubes," *Sci. Rep.*, vol. 7, no. 1, pp. 1–13,

[108] **H. Z. Geng, K. K. Ki, P. S. Kang, S. L. Young, Y. Chang, and H. L. Young,** (Jun. 2007). "Effect of acid treatment on carbon nanotube-based flexible transparent conducting films," *J. Am. Chem. Soc.*, vol. 129, no. 25, pp. 7758–7759,

[109] **D. W. Shin, J. H. Lee, Y. H. Kim, S. M. Yu, S. Y. Park, and J. B. Yoo,** (2009). "A role of HNO3 on transparent conducting film with single-walled carbon nanotubes," *Nanotechnology*, vol. 20, no. 47,

[110] **Y. Zhao and W. Li,** (2010). "Effect of annealing and HNO3-treatment on the electrical properties of transparent conducting carbon nanotube films," *Microelectron. Eng.*, vol. 87, no. 4, pp. 576–579,

[111] **A. Santidrián *et al.,*** (2019). "Chemical Postdeposition Treatments to Improve the Adhesion of Carbon Nanotube Films on Plastic Substrates," *ACS Omega*, vol. 4, no. 2, pp. 2804–2811,

[112] **A. Aldalbahi and M. Rahaman,** (2018). "Improvement in Electrode Performance of Novel SWCNT Loaded Three-Dimensional Porous RVC Composite Electrodes by Electrochemical Deposition Method,"

[113] **D. Janas,** (2018). "Powerful doping of chirality-sorted carbon nanotube fi lms," *Vaccum*, vol. 149, pp. 48–52,

[114] **B. Kumanek, T. Wasiak, G. Stando, P. Stando, D. Łukowiec, and D. Janas,** (2019). "Simple method to improve electrical conductivity of films made from single-walled carbon nanotubes," *Nanomaterials*, vol. 9, no. 8, pp. 1–11,

[115] **R. Jackson, B. Domercq, R. Jain, B. Kippelen, and S. Graham,** (2008). "Stability of doped transparent carbon nanotube electrodes," *Adv. Funct. Mater.*, vol. 18, no. 17, pp. 2548–2554,

[116] **C. K. Najeeb, J. H. Lee, J. Chang, and J. H. Kim,** (2011). "Evaluation of SOCl 2 doping effect on electrical conductivity of thin films of SWNTs and SWNT/PEDOT-PSS composites," *J. Nanosci. Nanotechnol.*, vol. 11, no. 7, pp. 5839–5844,

[117] **U. Dettlaff-Weglikowska *et al.,*** (2005). "Effect of SOCl2 treatment on electrical and mechanical properties of single-wall carbon nanotube networks," *J. Am. Chem. Soc.*, vol. 127, no. 14, pp. 5125–5131,

[118] **B. Dan, G. C. Irvin, and M. Pasquali,** (2009). "Continuous and Scalable Fabrication of Nanotube Films supp," *ACS Nano*, vol. 3, no. 4, pp. 835–843,

[119] **S. Devaraju *et al.,*** (2017). "Fabrication of durable and flexible single-walled carbon nanotube transparent conductive films," *RSC Adv.*, vol. 7, no. 31, pp. 19267–19272,

[120] **Y. H. Kim, C. Sachse, M. L. MacHala, C. May, L. Müller-Meskamp, and K. Leo,** (2011). "Highly conductive PEDOT:PSS electrode with optimized solvent and thermal post-treatment for ITO-free organic solar cells," *Adv. Funct. Mater.*, vol. 21, no. 6, pp. 1076–1081, Mar.

[121] **A. M. Nardes *et al.*,** (2007). "Microscopic understanding of the anisotropic conductivity of PEDOT:PSS thin films," *Adv. Mater.*, vol. 19, no. 9, pp. 1196–1200,

[122] **J. G. Tait *et al.*,** (2013). "Spray coated high-conductivity PEDOT:PSS transparent electrodes for stretchable and mechanically-robust organic solar cells," *Sol. Energy Mater. Sol. Cells*, vol. 110, pp. 98–106,

[123] **M. Yi, W. Jang, and D. H. Wang,** (2019). "Controlled pH of PEDOT:PSS for Reproducible Efficiency in Inverted Perovskite Solar Cells: Independent of Active Area and Humidity," *ACS Sustain. Chem. Eng.*, vol. 7, pp. 8245–8254,

[124] **F. Zhang, M. Johansson, M. R. Andersson, J. C. Hummelen, and O. Inganäs,** (2002). "Polymer photovoltaic cells with conducting polymer anodes," *Adv. Mater.*, vol. 14, no. 9, pp. 662–665,

[125] **S. Zhang, P. Kumar, A. S. Nouas, L. Fontaine, H. Tang, and F. Cicoira,** (2015). "Solvent-induced changes in PEDOT:PSS films for organic electrochemical transistors," *APL Mater.*, vol. 3, no. 1,

[126] **Y. J. Noh, S. S. Kim, T. W. Kim, and S. I. Na,** (2014). "Cost-effective ITO-free organic solar cells with silver nanowire-PEDOT:PSS composite electrodes via a one-step spray deposition method," *Sol. Energy Mater. Sol. Cells*, vol. 120, no. PART A, pp. 226–230,

[127] **X. Crispin *et al.*,** (2006). "2006_200_The Origin of the High Conductivity of (PEDOT−PSS) Plastic Electrodes.pdf," *Chem. Mater.*, vol. 18, no. 4, pp. 4354–4360,

[128] **J. Huang, P. F. Miller, J. S. Wilson, A. J. De Mello, J. C. De Mello, and D. D. C. Bradley,** (2005). "Investigation of the effects of doping and post-deposition treatments on the conductivity, morphology, and work function of poly(3,4- ethylenedioxythiophene)/poly(styrene sulfonate) films," *Adv. Funct. Mater.*, vol. 15, no. 2, pp. 290–296,

[129] **J. Luo *et al.*,** (2014). "Chemical post-treatment and thermoelectric properties of poly(3,4-ethylenedioxylthiophene):poly(styrenesulfonate) thin films," *J. Appl. Phys.*, vol. 115, no. 5,

[130] **J. S. Yeo *et al.*,** (2012). "Significant vertical phase separation in solvent-vapor-annealed poly(3,4-ethylenedioxythiophene):Poly(styrene sulfonate) composite films leading to better conductivity and work function for high-performance indium tin oxide-free optoelectronics," *ACS Appl. Mater. Interfaces*, vol. 4, no. 5, pp. 2551–2560,

[131] **J. Ouyang, C. W. Chu, F. C. Chen, Q. Xu, and Y. Yang,** (2005). "High-conductivity poly(3,4-ethylenedioxythiophene):poly(styrene sulfonate) film and its application in polymer optoelectronic devices," *Adv. Funct. Mater.*, vol. 15, no. 2, pp. 203–208,

[132] **X. Crispin *et al.*,** "Stability of Poly (3 , 4-ethylene dioxythiophene)– Poly (styrene sulfonate): A Photoelectron Spectroscopy Study," *Polymer (Guildf).*, pp. 2561–2583.

[133] **M. Döbbelin *et al.*,** (2007). "Influence of ionic liquids on the electrical conductivity and morphology of PEDOT:PSS films," *Chem. Mater.*, vol. 19, no. 9, pp. 2147–2149,

[134] **I. Cruz-Cruz, M. Reyes-Reyes, M. A. Aguilar-Frutis, A. G. Rodriguez, and R. López-Sandoval,** (2010). "Study of the effect of DMSO concentration on the thickness of the PSS insulating barrier in PEDOT:PSS thin films," *Synth. Met.*, vol. 160, no. 13–14, pp. 1501–1506,

[135] **G. Zotti *et al.*,** (2003). "Electrochemical and XPS studies toward the role of monomeric and polymeric sulfonate counterions in the synthesis, composition, and properties of poly(3,4-ethylenedioxythiophene)," *Macromolecules*, vol. 36, no. 9, pp. 3337–3344,

[136] **C. S. Suchand Sangeeth, M. Jaiswal, and R. Menon,** (2009). "Correlation of morphology and charge transport in poly(3,4-ethylenedioxythiophene)-polystyrenesulfonic acid (PEDOT-PSS) films," *J. Phys. Condens. Matter*, vol. 21, no. 7,

[137] **E. J. Lee, M. H. Chang, Y. S. Kim, and J. Y. Kim,** (2013). "High-pressure polyol synthesis of ultrathin silver nanowires: Electrical and optical properties," *APL Mater.*, vol. 1, no. 4,

[138] **M. B. Gebeyehu, T. F. Chala, S. Y. Chang, C. M. Wu, and J. Y. Lee,** (2017). "Synthesis and highly effective purification of silver nanowires to enhance transmittance at low sheet resistance with simple polyol and scalable selective precipitation method," *RSC Adv.*, vol. 7, no. 26, pp. 16139–16148,

[139] **S. Ye, A. R. Rathmell, Z. Chen, I. E. Stewart, and B. J. Wiley,** (2014). "Metal nanowire networks: The next generation of transparent conductors," *Adv. Mater.*, vol. 26, no. 39, pp. 6670–6687,

[140] **D. Li and Y. Xia,** (2004). "Electrospinning of nanofibers: Reinventing the wheel?," *Adv. Mater.*, vol. 16, no. 14, pp. 1151–1170,

[141] **V. trinh Pham *et al.*,** (2017). "Effect of organic solvents on the properties of DWCNT/PEDOT:PSS transparent conductive films," pp. 0–20,

[142] **Z. Z. Gu *et al.*,** (2019). "Highly conductive sandwich-structured CNT/PEDOT:PSS/CNT transparent conductive films for OLED electrodes," *Appl. Nanosci.*, vol. 9, no. 8, pp. 1971–1979,

[143] **B. D. Martin *et al.*,** (2004). "Hydroxylated secondary dopants for surface resistance enhancement in transparent poly(3,4-ethylenedioxythiophene)-poly(styrenesulfonate) thin films," *Synth. Met.*, vol. 142, no. 1–3, pp. 187–193,

[144] **S. Timpanaro, M. Kemerink, F. J. Touwslager, M. M. De Kok, and S. Schrader,** (2004). "Morphology and conductivity of PEDOT/PSS films studied by scanning-tunneling microscopy," *Chem. Phys. Lett.*, vol. 394, no. 4–6, pp. 339–343,

[145] **W. H. Kim, A. J. Mäkinen, N. Nikolov, R. Shashidhar, H. Kim, and Z. H. Kafafi,** (2002). "Molecular organic light-emitting diodes using highly conducting polymers as anodes," *Appl. Phys. Lett.*, vol. 80, no. 20, pp. 3844–3846,

[146] **V. A. Online,** (2013). "Annealing-free, fl exible silver nanowire – polymer composite electrodes via a continuous two-step spray-coating method," pp. 977–983,

[147] **X. Y. Zeng, Q. K. Zhang, R. M. Yu, and C. Z. Lu,** (2010). "A new transparent conductor: Silver nanowire film buried at the surface of a transparent polymer," *Adv. Mater.*, vol. 22, no. 40, pp. 4484–4488,

[148] **W. Gaynor, G. F. Burkhard, M. D. McGehee, and P. Peumans,** (2011). "Smooth nanowire/polymer composite transparent electrodes," *Adv. Mater.*, vol. 23, no. 26, pp. 2905–2910,

CURRICULUM VITAE

Name Surname **:** Serra Melek AKYÜZ

EDUCATION

- **B.Sc.** **:** 2017, Marmara University, Faculty of Engineering, Department of Chemical Engineering

PROFESSIONAL EXPERIENCE AND REWARDS:

- Research Assistant, Turkish – German University, Faculty of Science, Energy Science and Technology (2021-Present)
- Scientific Researcher, TÜBİTAK Bilateral Cooperation Project with Korea Title: Cost-effective production of perovskite and near-infrared sensitive quantum dot solar cells with carbon electrode and newly designed organic-inorganic hybrid hole transport layer (2019-2021)